

The A.D. 900–930 Seattle-Fault-Zone Earthquake with a Wider Coseismic Rupture Patch and Postseismic Submergence: Inferences from New Sedimentary Evidence

by Maria E. Martin Arcos

Abstract Stratigraphic evidence for coseismic uplift, a tsunami, and a sandy debris flow linked to the A.D. 900–930 Seattle-fault-zone earthquake and subsequent submergence is present at Gorst at the terminus of Sinclair Inlet, Washington. This study indicates that at least 3 m of uplift preceded a tsunami followed by a sandy debris flow. Though the Seattle and Tacoma fault zones ruptured within the error of ages of the tsunami deposit, model simulations indicate the Seattle fault generates an order of magnitude larger tsunami in the vicinity of the field area than the Tacoma fault and is the more likely generator of the tsunami. Simulations indicate amplitude from a Seattle-fault-zone-generated wave train was 4–5 m, and stratigraphy shows the tsunami left a sandy deposit. Soft-sediment deformation narrows the time window for the debris flow to the hours to months after the tsunami. Slope failure in unconsolidated glacial sands likely initiated a debris flow that surged at least 2 km down Gorst Creek valley and left a more than 40-cm-thick deposit along the creek and in the wetlands. Submergence of a *Thuja plicata* (western red cedar) swamp into the intertidal zone indicates at least 1.5 m of submergence in the last 1100 years. This submergence indicates uplift on nearby marine terraces associated with the Seattle fault zone was likely higher, and the A.D. 900–930 earthquake was potentially larger, than previously recognized.

Introduction

The Seattle fault zone, a series of active east–west trending thrust faults, poses a seismic threat to the Puget Sound region (Fig. 1). The fault zone has only one known large earthquake, A.D. 900–930 (Atwater, 1999) and no large historical events (Ludwin *et al.*, 1991). Geological records of prehistorical events are the only clues to the earthquake potential of the fault.

The coastal marsh at Gorst is a potential recorder of tsunamis, slope failure triggered by earthquakes, and land-level changes (Figs. 1, 2). Strategically for studies of the Seattle fault, Gorst lies to the south and west of the previously mapped evidence of the A.D. 900–930 Seattle-fault-zone earthquake, uplifted bedrock terraces (Fig. 1). Advantageously for hazard assessment, Gorst is located less than 4 km from Bremerton and its naval base.

This study identifies evidence for uplift in coastal marsh facies farther south and west than deformation predicted by current fault models. Further, two other kinds of stratigraphic evidence for a paleoearthquake, tsunami, and debris-flow deposit (Fig. 1) extend the geographic record of the A.D. 900–930 earthquake. In addition, evidence of submergence since the A.D. 900–930 earthquake indicates the earth-

quake deformation was broader and higher than previously mapped.

Puget Lowland Quaternary History

Pleistocene glacial ice sheets modified the Puget lowland and obscured portions of the geological history of the region. The last glaciation, the Fraser glaciation, reached its peak in the Vashon stade ~15 ka (Booth, 1994). The Fraser glaciation emplaced glacial till, lacustrine, advance, and outwash deposits. Glacial ice sheets, from the last and prior glaciations, concealed the long-term seismic history of the area by beveling the landscape and blanketing much of the lowland with Pleistocene deposits, masking offset along faults.

After the retreat of the ice sheets, the region's sea level rise tapered off ~5000 years ago (Dragovich *et al.*, 1994; James *et al.*, 2009), but other factors induced relative sea level variations in the Holocene. The majority of isostatic rebound from glacial ice sheets was completed by 9,000–10,000 years ago due to the low viscosity of the mantle below the Puget lowland (James *et al.*, 2000). Peat records demonstrate other relative sea level variations from sea level rise and tectonic deformation. Stratigraphy from northern

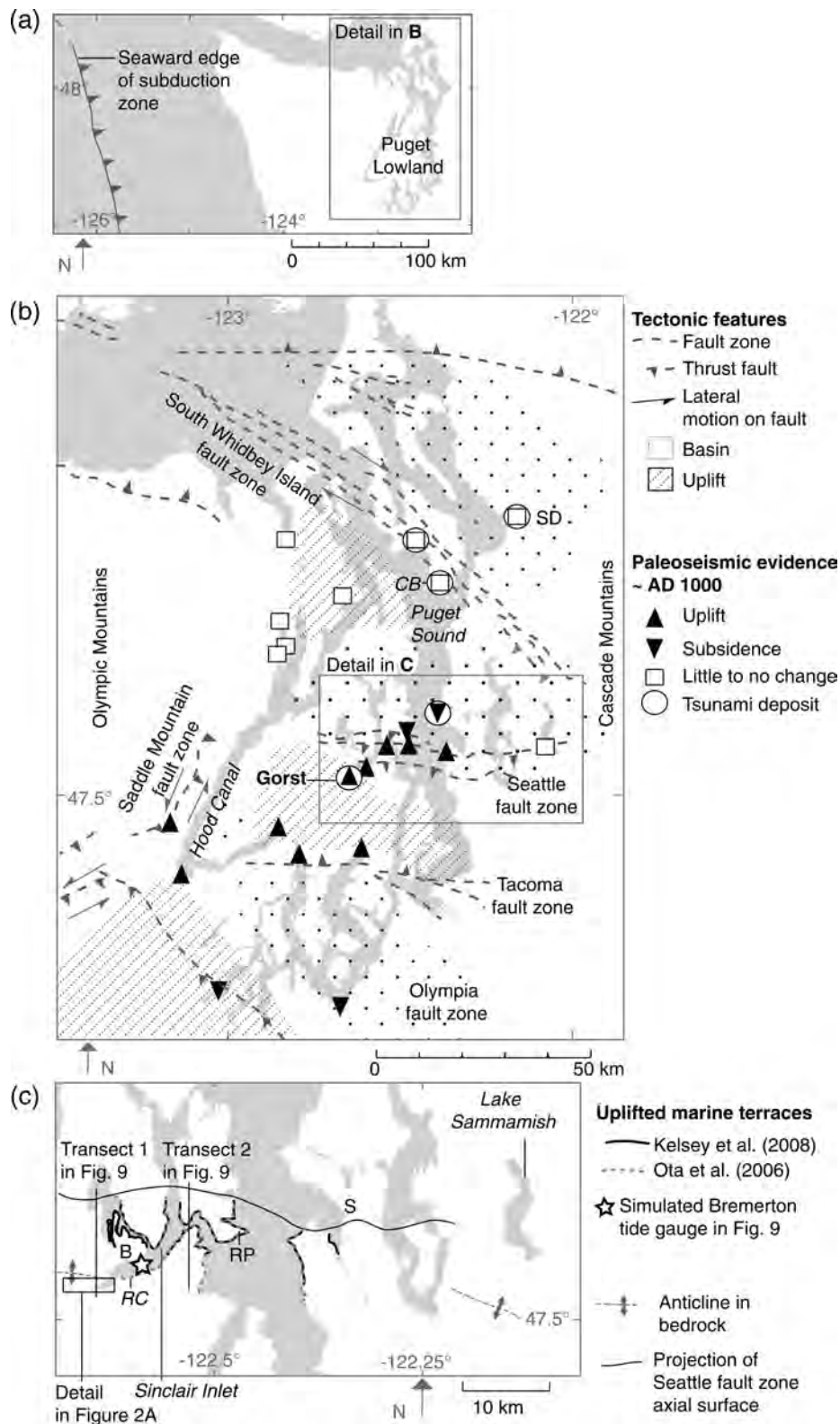


Figure 1. Maps of the tectonic setting of the Puget lowland. (a) Map of Cascadia subduction zone and coastline. (b) Map of the Puget lowland showing active faults and locations of paleoseismic studies modified from Blakely *et al.* (2009); tsunami data from Atwater and Moore, 1992 and Bourgeois and Johnson, 2001; land-level data from Eronen *et al.*, 1987; Beale, 1990; Bucknam *et al.*, 1992; Williams and Hutchinson, 2000; Sherrod, 2001; Williams *et al.*, 2005; and Martin, 2011. (c) Location of mapped marine terraces associated with the A.D. 900–930 Seattle-fault-zone earthquake (Ota *et al.*, 2006; Kelsey *et al.*, 2008); B, Bremerton; RC, Ross Creek; RP, Restoration Point; S, Seattle; SD, Snohomish Delta. Projection of axial surface of Seattle fault zone from Kelsey *et al.* (2008).

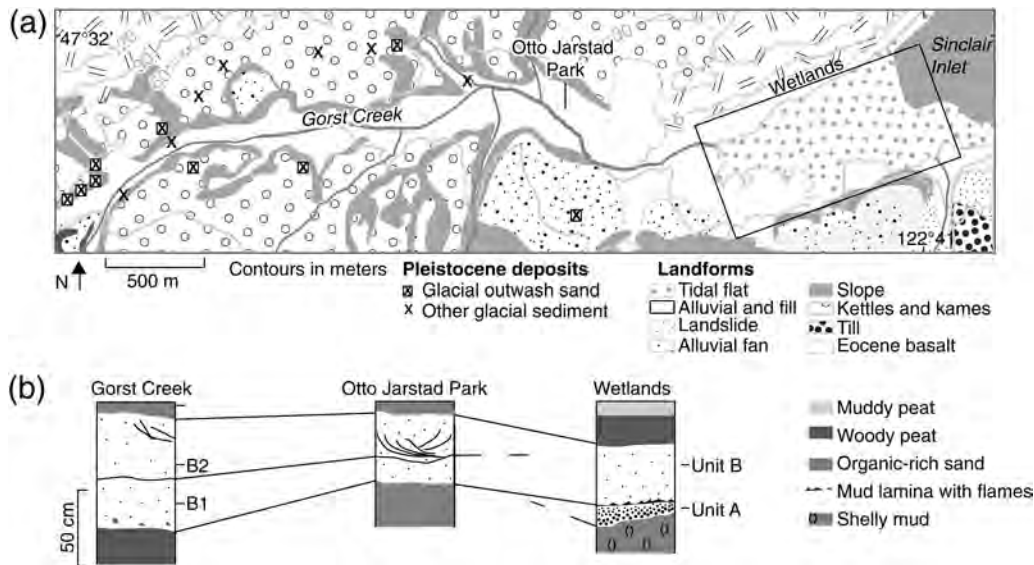


Figure 2. Map and generalized stratigraphic sections from Gorst. (a) Geomorphic map of the Gorst Creek drainage and wetlands showing Pleistocene glacial outcrops and main areas of the field study. Map modified from Haugerud (2009). Wetlands refers to swamps and marshes beside tidal flat. (b) Generalized sections from the field areas with main units.

Hood Canal shows a gradual relative sea level rise of about 6 m the last 6000 years with less than 1 m of the rise in the last 1000 years (Eronen *et al.*, 1987). Beale (1990) worked at six marshes in the northern Puget lowland and found a similar, less than 1-m sea level rise in the last 1000 years. Historical records in eastern Puget Sound show more variability. Using almost 100 years of tide gauge records, Holdahl *et al.* (1989) interpreted 1–2-mm submergence a year near Gorst, yet Verdonck (2006) found no evidence for submergence also using tide gauges. Compiling a variety of geologic records, Shipman (1989) predicted submersion of 1 mm/yr in the area around Gorst.

Several mostly east–west-trending faults run beneath the Puget lowland. Though none has generated a large ($M_w > 7$) historical (since ~1850) earthquake, they have generated large Holocene earthquakes (Ludwin *et al.*, 1991; Bucknam *et al.*, 1992; Sherrod, 2001; Sherrod *et al.*, 2004). Rupture on multiple faults about 1100 years ago generated a wide variety of geological records in the Puget lowland. The Seattle, Olympia, Tacoma, and Saddle Mountain fault zones show evidence for rupture during this time period (Bucknam *et al.*, 1992; Sherrod, 2001; Sherrod *et al.*, 2004; Blakely *et al.*, 2009; Fig. 1). The Tacoma-fault-zone earthquake generated widespread land changes, liquefaction, and likely a tsunami (Sherrod *et al.*, 2004; Venturato *et al.*, 2007; Martin and Bourgeois, 2012). The Seattle fault zone has received the most attention due to a widespread record of the A.D. 900–930 earthquake and the fault trend running under the Seattle metropolitan area.

Seattle Fault Zone

Seismic reflection, uplifted bedrock, and evidence of an earthquake A.D. 900–930 locate the Seattle fault zone

(Gower *et al.*, 1985; Atwater and Moore, 1992; Bucknam *et al.*, 1992; Johnson *et al.*, 1999, Haeussler and Clark, 2000; Fig. 1). Near the main arm of Puget Sound, seismic reflection surveys (Johnson *et al.*, 1999) and coseismic deformation from a large fault rupture A.D. 900–930 (Bucknam *et al.*, 1992; Nelson *et al.*, 2003; ten Brink *et al.*, 2006; Kelsey *et al.*, 2008) trace the Seattle fault zone. The A.D. 900–930 earthquake, estimated to have been M_w 7.0–7.5 (ten Brink *et al.*, 2006) uplifted marine terraces along Puget Sound (Bucknam *et al.*, 1992; Ota *et al.*, 2006; Kelsey *et al.*, 2008; Fig. 1c). To the east the Seattle fault zone is traced east of Lake Sammamish where it possibly interacts with the South Whidbey Island fault zone (Liberty and Pratt, 2008). To the west, uplifted bedrock near Gorst (Haeussler and Clark, 2000; Fig. 2, Eocene basalt) indicates the Seattle fault zone extends into this region.

Several uncertainties remain about the extent of the Seattle fault zone and about the specifics of a fault rupture A.D. 900–930 (Kelsey *et al.*, 2008; Liberty and Pratt, 2008). (1) There is no consensus on the specific structure of the fault though most models include a main, blind-thrust fault with back thrusts, which reach the surface in some locations (Pratt *et al.*, 1997; Johnson *et al.*, 1999; Blakely *et al.*, 2002; Brocher *et al.*, 2004; ten Brink *et al.*, 2006; Kelsey *et al.*, 2008; Liberty and Pratt, 2008). (2) The western extent of the Seattle fault is unknown, but recent studies have attempted to trace it across Hood Canal (Karel *et al.*, 2008; Blakely *et al.*, 2009). (3) Beyond the extent of the uplifted marine terraces, the zone of deformation associated with the A.D. 900–930 earthquake is not well mapped. To the east, no evidence of surface rupture has been found on faults near the western shores of Lake Sammamish (Sherrod, 2002), though movement on the blind thrust is possible in this area. To the west, no evidence of coseismic deformation has been published previous to this study, which

traces influence of the A.D. 900–930 event several kilometers west and south of the mapped terraces (Fig. 1c).

Land-Level Changes, Tsunamis, and Debris Flows in the Puget Lowland

Previous studies of coseismic land-level change in the Puget lowland have successfully used stratigraphy and macro- and microfossil changes to document Holocene fault movements. Bucknam *et al.* (1992) used both abrupt facies changes in marsh stratigraphy and uplifted marine terraces in several sites in the central Puget lowland as evidence for earthquakes 1100 years ago. Delta and marsh stratigraphy in the southern Puget lowland also reveals evidence for facies changes linked to fault rupture (Sherrod, 2001; Barnhardt and Sherrod, 2006). On the Snohomish delta north of Seattle, Bourgeois and Johnson (2001) interpreted abrupt facies changes as evidence of local subsidence due to strong shaking, rather than to fault-induced subsidence.

The Puget lowland experienced historical and paleotsunamis. Historical tsunamis such as the 1-m–2-m 1949 tsunami near Tacoma (Chleborad, 1994) have all been landslide-generated, small, and local. The best-studied evidence of a paleotsunami in the Puget lowland is a sand layer, likely left by a tsunami from the A.D. 900–930 Seattle-fault earthquake (Atwater and Moore, 1992; Bourgeois and Johnson, 2001; Fig. 1).

Prior work in the Puget lowland has focused on historic and prehistoric slope failures and debris flows generated by weather, and by tectonic and volcanic activity. Most historic cases are linked to unconsolidated glacial deposits and prolonged winter rainy seasons that along with steep slopes make the region prone to landslides (Thorson, 1989; Shipman, 2001). In the geological record, landslides and turbidity currents in lakes, and rock falls in the Olympic Mountains have been linked to fault ruptures about 1100 years ago (Karlin and Abella, 1992; Schuster *et al.*, 1992; Logan *et al.*, 1998). However, the largest and best-understood debris-flow deposits in the Puget lowland are from Cascade-volcano lahars (e.g., Pierson and Scott, 1985).

Gorst

The geology of the Gorst Creek drainage shows evidence of both long-term uplift and glacial overprinting. Uplifted Eocene basalts crop out to the north of the Gorst Creek drainage and Sinclair Inlet (Haugerud, 2009; Fig. 2). The basalts are part of the bedrock of the Seattle uplift, one of a series of uplifts and basins in the Puget lowland (Fig. 1). Blanketing the basalt are unconsolidated deposits of the last glacial maximum. Outwash sands and dead-ice deposits abound along the Gorst Creek drainage (Fig. 2). In many areas surrounding Gorst, landslides and slope failures have reworked the glacial deposits (Haugerud, 2009; Fig. 2).

The Gorst locality consists of three main modern environments: the forest and alluvial plain along Gorst Creek, the urbanized zone between Otto Jarstad Park and Sinclair Inlet,

and the alder swamp and salt marsh of the wetlands (Fig. 2). Another environment, an extensive muddy intertidal zone, lies at the end of Sinclair Inlet in part due to a spring-tide range of 3.58 m as measured at the tide gauge at Bremerton (Mofjeld *et al.*, 2002).

Methods

At Gorst, the quantification of land-level change relative to sea level used a combination of field surveys and lab analysis, with results compared with modern analogs. Each site was located using a hand-held GPS and was plotted onto a geo-referenced map (Fig. 3). In conjunction with the relative sea level work, this study mapped two anomalous sand deposits at a stratigraphic contact indicating uplift (relative sea level drop). Additionally, tsunami modeling estimated the timing and magnitude of events.

Radiocarbon ages helped to correlate the stratigraphic units to other events in the Puget lowland. Material from outcrops was subsampled in the field and lab and sent to Beta Analytic or the National Ocean Sciences Accelerator Mass Spectrometry Facility for radiocarbon dating. A marine reservoir correction of 400 years was used for the age on the bivalve shell (Deo *et al.*, 2004).

Relative Sea-Level Change

The record of land-level change in Gorst stratigraphy was quantified using a combination of field survey of modern vegetation, delineation of stratigraphy, and lab analysis of macrofossils. Key indicators of land elevation relative to sea level are stratigraphic changes in sedentary organisms such as nestling clams and rooted vegetation. To quantify the relationship of paleo- to modern vegetation, this study measured a topographic profile using a transit and hand level and then mapped modern vegetation along the profile (Fig. 4) to compare with macrofossils in peat samples. For this profile, this study used species-cover abundance to characterize different vegetation zones, with the vegetation zones of Sherrod (1999) serving as a basis for grouping the data from Gorst. Profile elevation relative to NAVD88 0 was calculated by comparing the time and sea level when the profile was measured with the sea level at the Bremerton tide gauge.

Macrofossils of plants and mollusks from different stratigraphic units characterized the ancient environments. Macrofossils content of all cores and outcrops were noted in the field. For five sites, the outcrop was subsampled in the field, and then samples were picked and macrofossils were identified under a binocular microscope in the lab. For identification, this study used botanical reference collections from the University of Washington biology department and faunal reference collections from the University of Washington Burke Museum.

Sandy Deposits

In order to interpret the mode of deposition of the sandy deposits that in places split at the shelly-mud-woody peat

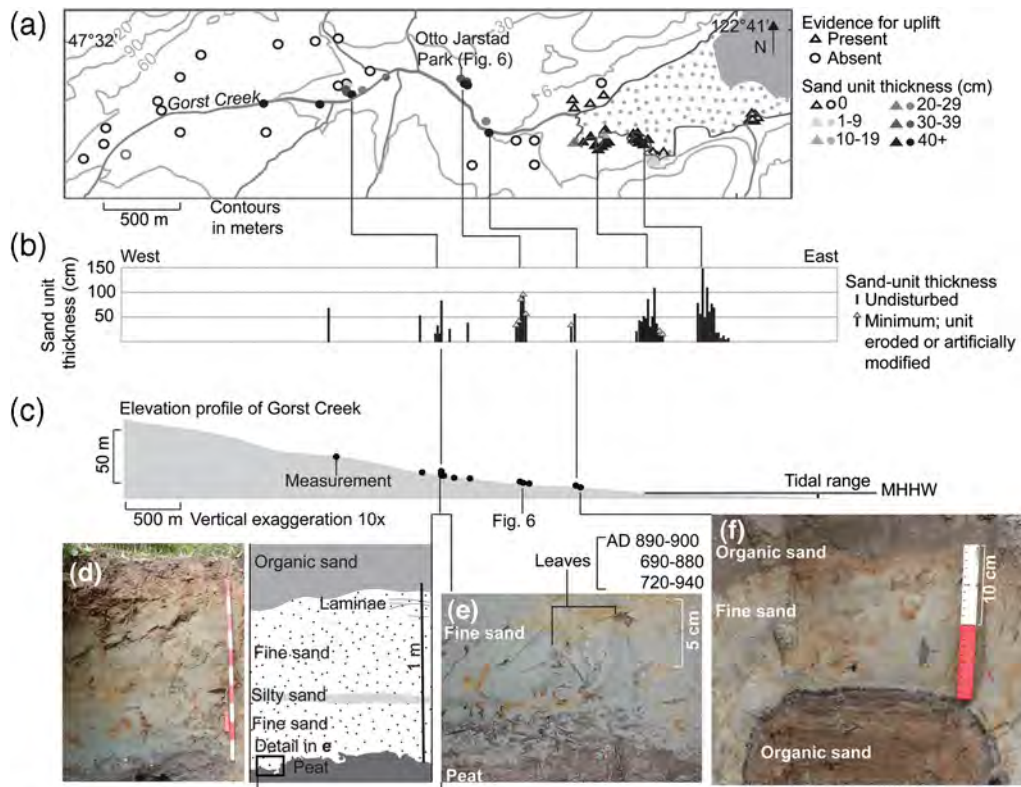


Figure 3. Sand thickness along Gorst Creek showing unit B is only present along Gorst Creek. (a) Map of thickness variation. (b) Total thickness of sand unit (A and B where both are present) along Gorst Creek and in wetlands. (c) Profile along Gorst Creek showing measurement locations. (d) Photograph of deposit from an outcrop along Gorst Creek. (e) Detail of well-preserved leaves entrained in sand deposit. (f) Detail of sand deposit near Gorst Creek. In this location the top of the deposit was removed in historical times. The color version of this figure is available only in the electronic edition.

contact, this study mapped the two sand bodies and described their internal characteristics, both in outcrop and in the subsurface (Fig. 3). Peat-, auger-, and vibra-coring, as well as hand-dug excavations and backhoe trenches revealed the stratigraphy. This work resulted in over 100 stratigraphic sections (Fig. 3). Where possible excavations and cleaned cut banks were used observe the sedimentary structures and variability within the deposit. Sedimentary peels of excavation walls and sampled monoliths exposed sedimentary structures in the sandy deposits (e.g., Fig. 5e,f).

Grain-size analysis aided the comparison of sandy deposits with various sedimentary sources. Grain size was measured using a settling column. In the studied sections, samples were taken at 1-cm intervals from outcrops in the field and monoliths in the lab. In addition, bulk grain-size samples from various glacial outcrops and the creek bed were compared with the sandy deposits in question.

Tsunami Modeling

In order to simulate the hypothesized paleotsunami from about 1100 years ago, this study used standard methods for establishing fault parameters and for modeling tsunamis. Sea-floor deformation was created from fault parameters using a model based on Okada (1985). Modeling of Seattle

and Tacoma fault scenarios used GeoClaw (LeVeque and George, 2008; LeVeque *et al.*, 2011; Berger *et al.*, 2011). This forward model uses shallow-water-wave equations and adaptive-grid refinement to simulate tsunami waves across bathymetry and onto topography. The input of bottom friction in the form of Manning's formula used a coefficient of 0.025.

Model simulations used the combined bathymetry and topography of the Puget lowland by Finlayson (2005). The finest grid-cell size used was 0.0006875 degrees square ($\sim 76 \text{ m} \times 52 \text{ m}$). Modern bathymetry and topography was used for simulations because the paleobathymetry is not well enough understood to use for this problem.

Observations and Interpretations

Field Area

There are three main study areas in the Gorst locality (Fig. 2). The wetland fringes Sinclair Inlet and consists of modern salt marsh and freshwater swamp. Otto Jarstad Park is a former homestead site along Gorst Creek that is now a Bremerton city park. This study refers to the area upstream of Otto Jarstad Park as the Gorst Creek area. In each of these areas was the location of many stratigraphic sections. The

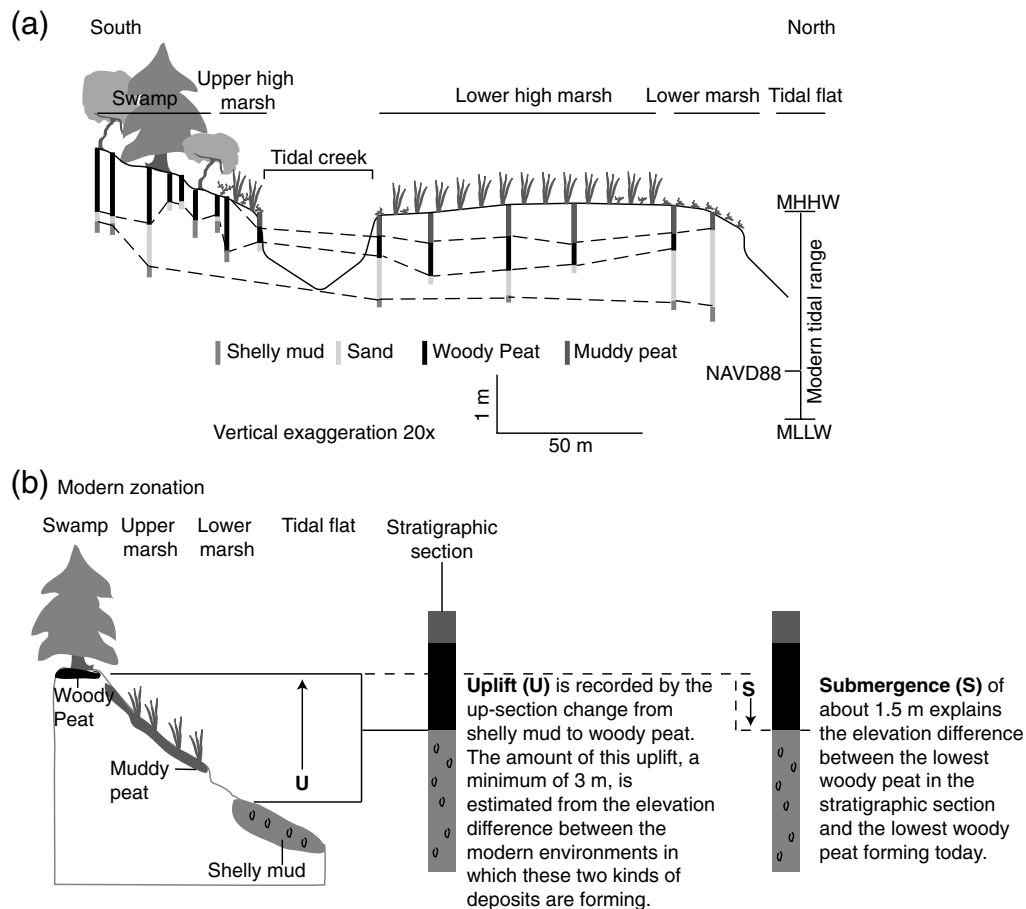


Figure 4. Modern environments and quantification of relative land-level change. (a) Topographic profile across Gorst marsh (location in Fig. 2) detailing modern vegetation zones taken from Sherrod (1999) and stratigraphy. Bar to the left shows intertidal range between mean higher high water (MHHW) and mean lower low water (MLLW). (b) Cartoons of stratigraphic and environmental elevations used in the quantification of land-level change.

general stratigraphy in the wetlands is of a basal sandy mud draped by sandy units and overlying woody peat. Along Gorst Creek a sandy unit is both over- and underlain by either peat or organic-rich sand.

Evidence for Relative Sea-Level Change

Observations

The difference in elevation between modern intertidal mudflat devoid of vegetation and the lowest trees and salt-intolerant vegetation is 0.9–1.1 m (Fig. 4), a value in agreement with other vegetation profiles in the Puget lowland that found values of 1.2–1.5 m (Sherrod, 1999; Sherrod, 2001).

In stratigraphic sections, the basal sandy mud contains articulated bivalves and other shells (Table 1). Typically, the top 10–20 cm of the mud unit does not contain shells, possibly due to dissolution by acidic groundwater from the overlying peat. The shells indicate a lower intertidal environment (Kozloff, 1983; M. Dethier, personal communication, 2010).

The dark brown woody peat overlying the (sandy units and) shelly-mud contains macrofossils of *Thuja plicata* (western red cedar), including *in-situ* trunks protruding from

the marsh surface, and other swamp-forest species (Table 1). The lowest occurrence of this woody peat occurs 1.5 m below the lowest modern trees (Fig. 4). A similar change from mud containing shells to freshwater peat also occurs at Ross Creek (Fig. 1), 3 km down inlet from Gorst, though no sand layer is present at this location.

The woody peat has a sharp to gradational upper contact with a muddier peat containing salt-tolerant species including *Triglochin maritimum* (arrow grass) leaf bases, and *Distichlis spicata* (salt grass) rhizomes.

A bivalve shell from the top 5 cm of the basal sandy mud unit had a corrected radiocarbon age of A.D. 790–1050 (Table 2). A *Tsuga heterophylla* cone from the basal 2 cm of the woody peat had an age of A.D. 1240–1390 (Table 2; Fig. 5).

Interpretation

Facies changes confirmed by macrofossils indicate the Gorst marsh site was uplifted at least 3 m approximately 1100 years ago and then later subsided. Macrofossil content in the sandy mud compared with the overlying woody peat

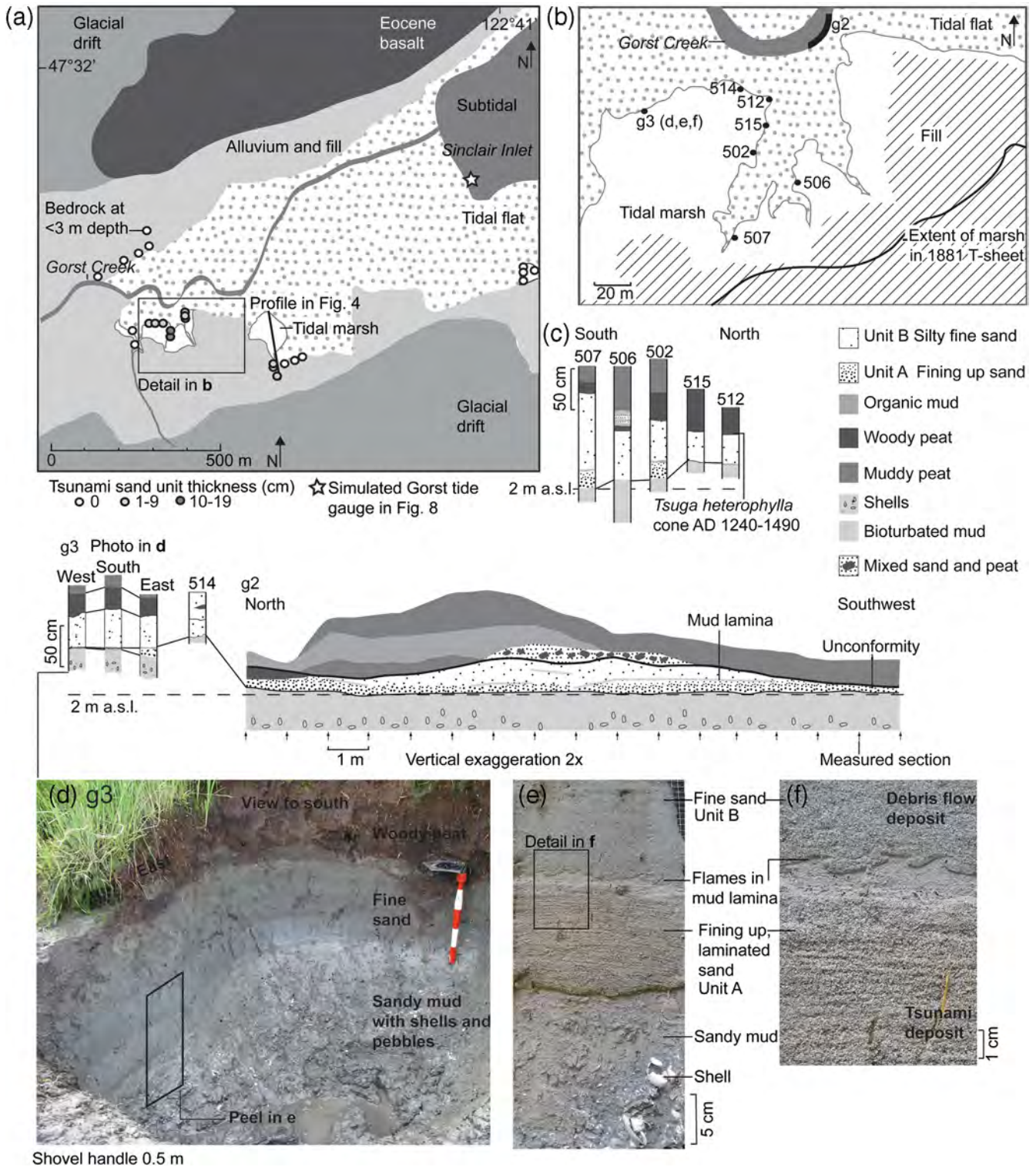


Figure 5. Maps, stratigraphic sections, and photographs of the Gorst wetlands area detailing the relatively consistent thickness of unit A relative to unit B. (a) Map of wetlands including thickness of unit A. (b) Unit A thickness and outcrop locations in Gorst wetlands. (c) Stratigraphic detail of outcrops. (d) Details of sedimentary structure from outcrop. Painted sections on shovel are in 10-cm increments. (e) Sediment peel from outcrop in (d). (f) Detail of sedimentary peel in (e). The color version of this figure is available only in the electronic edition.

indicates an environmental change from lower intertidal to cedar swamp or forest (Table 1). In the modern environment, the minimum elevation difference between trees and the

lower intertidal is approximately 3.5 m (Fig. 4). This study conservatively estimates a minimum uplift of 3 m because of fossil-free deposits about 0.5-m thick between

Table 1
Marine Shells and Plant Macrofossils*

Unit	Species	Common Name
Sandy mud [†]	<i>Euspira lewisii</i>	Moon snail
	<i>Lottia pelta</i>	Limpet
	<i>Nassarius mendicus</i>	Lean basket-whelk
	<i>Nucella lamellosa</i>	Friiled dogwinkle
	<i>Macoma nasuta</i>	Bent nosed clam
	<i>Mytilus trossulus</i>	Mussel
	<i>Ostreola conchaphilia</i>	Olympia oyster
	<i>Clinocardium nuttallii</i>	Heart cockle
Woody peat	<i>Saxidomus gigantea</i>	Butter clam
	<i>Thuja plicata</i>	Western red cedar
	<i>Tsuga heterophylla</i>	Western hemlock
Muddy peat	Apiaceae seeds	
	<i>Triglochin maritimum</i>	Common arrowgrass
	<i>Distichlis spicata</i>	Salt grass

*Shells present in basal marine mud indicate lower intertidal environment, and plant macrofossils from woody peat indicate swamp environment. Shells are from the base of the g2 outcrop (Fig. 4).

[†]E. Nesbitt of the Burke Museum aided in identifying the shells.

the shelly-mud and the forest peat. This value is a minimum because the mollusks' habitat extends for at least a meter below the upper elevation used in this calculation, and cedar forests extend many meters above their lowest limit used in this calculation.

Rapid uplift generated the change from intertidal to forest environment. This facies change is not due to sea level drop because there are no records of a rapid eustatic or Puget Sound basin sea level drop in the last 1500 years; instead sea level has been rising in this time (Clague *et al.*, 1982; Eronen *et al.*, 1987; Beale, 1990; Dragovich *et al.*, 1994). The interpretation of rapid uplift is based further on the sharp contact of the woody peat and sandy mud unit (where intervening sand is absent) and the stratigraphic skipping of salt-marsh

facies expected in a normal prograding sequence. If the wetland's change from intertidal to freshwater was gradual, deposits from the lower and upper marsh environments would be expected in the stratigraphy as the area slowly emerged into progressively fresher-water environments. However, woody peat always overlies the shelly-mud, and the only intervening deposits are tsunami and debris flow, not muddy marsh deposits.

Since the time of this uplift, the area has experienced submergence; in some locations, the cedar-forest-peat is now eroding out into the intertidal zone. The difference in elevation between the lowest woody peat in cores and the modern equivalent environment is 1.5 m (Fig. 4), indicating at least this much submergence since the abrupt uplift event. It is unclear if this submergence was rapid or gradual. Because the contact between the woody peat and muddy peat is not always sharp and because the contact is between two adjacent facies in the modern environment, it is difficult to determine the rate of submergence.

Tsunami and Debris-Flow Deposits

Observations

Two kinds of sand deposits intervene between the shelly-mud–forest-peat contact in the wetlands along Sinclair Inlet (Fig. 5), and the upper of these deposits can be traced in cut banks and cores along Gorst Creek. In wetlands sections, a silty sand deposit up to 1.6-m-thick (Fig. 5) lies at the abrupt facies change from sandy, shelly-mud to peat (Figs. 4, 6). The sand has a sharp basal contact and a sharp to gradational contact with overlying peat. The deposit in the wetlands typically contains two units. The lower unit, unit A, fines upward from medium and coarse sand and pebbles to fine sand and silt, in places capped by a thin, discontinuous mud lamina. Unit A is overlain by unit B, a deposit dominated by silty, fine to medium sand. A third unit, unit C, is

Table 2
Radiocarbon Ages from Gorst

Measured, 0000 ¹⁴ C yr B.P.	Calibrated 2 Sigma Range, A.D.*	Limiting Age	Material	Location; Latitude, Longitude	Laboratory and Sample Number [†]
1540 ± 70	790–1050	Limiting maximum for unit A and B	Shell in mud 5 cm below sand units	Wetland; 47.526528, –122.692889	BETA 263044
700 ± 40	1240–1390	Limiting minimum for unit A and B	<i>Tsuga heterophylla</i> cone in 2 cm above sand units	Wetland; 47.52655, –122.69600	BETA 263042
1390 ± 40	570–690	Limiting maximum for unit B	Charcoal in 5 cm below unit B	Otto Jarstad Park; 47.530485, –122.708573	BETA 263043
1100 ± 25	890–990	Limiting maximum for unit B	Leaf in basal 5 cm of unit B	Along Gorst Creek; 47.52988, –122.71923	NOSAMS 78396
1240 ± 30	690–880	Limiting maximum for unit B	Leaf in basal 5 cm of unit B	Along Gorst Creek; 47.52988, –122.71923	NOSAMS 78395
1190 ± 30	720–940	Limiting maximum for unit B	Leaf in basal 5 cm of unit B	Along Gorst Creek; 47.52988, –122.71923	NOSAMS 78394

*Calendar age was calibrated using IntCal 09 (Reimer *et al.*, 2009) using the online program OxCal (Data and Resources).

[†]Samples were processed by Beta Analytic (BETA) and National Ocean Sciences Accelerator Mass Spectrometry Facility (NOSAMS). The shell age has a marine reservoir correction of 400 years (Deo *et al.*, 2004).

found only in the wetlands. It differs from units A and B in both sedimentary structures and grain size.

Unit A

1 Unit A is characterized by normal grading, typically fining from coarse sand and pebbles upward to fine sand. It is found only in the wetlands. Of the 75 measured sections in the wetlands, in 23 unit A and B are distinct units separated by a mud lamina (Fig. 5). The mud lamina caps unit A in some sites and is less than 0.5 cm thick. In one site, (Fig. 5e) the mud lamina is deformed into flame structures 0.5–1.5 cm high. Where the lamina is not present, the similar grain sizes of unit B and the upper portion of unit A make the contact difficult to distinguish, especially in cores.

Where possible to measure, unit A is typically 5–7-cm thick and up to 24-cm thick. It is thickest in lower-elevation sites and is observed to thicken into depressions, for example, in the g3 excavation (Fig. 5). In some sites, the sand fills invertebrate burrows into the lower muddy unit. Pebbles in the deposit consist of lithics or rounded mud clasts similar to clasts in the modern tidal channels. This study found no suitable material for radiocarbon dating in unit A.

Unit B

A typically massive basal deposit (unit B1) overlain by laminae and cut-and-fill structures (unit B2) characterize unit B. Unit B extends upstream along Gorst Creek for at least 2 km (Fig. 3). Based on 14 cores and cut banks and three backhoe trenches along Gorst Creek, the deposit remains > 50 cm thick except for where it has been cut into by human activity. In the wetlands, unit B is over a meter thick in some locations but typically is 30–40-cm thick (Fig. 5). In general, unit B thins and becomes patchier perpendicular to Gorst Creek, up the side of the valley, and at higher elevations (Fig. 4; Fig. 6, trench 3). Of the three backhoe trenches at Otto Jarstad Park, in the one closest to the slope (trench 3) the deposit is thinner and patchier than in the other two trenches.

In the wetlands, the sedimentary structure of the deposit is mostly massive (B1), though in some locations the unit contains one or more laminae in the upper portion. At Otto Jarstad Park, the basal 5–8 cm of the deposit (B1) is massive fine sand and silt with rare soft-sediment clasts. Unit B1 has a sharp upper contact with B2, a fine to medium sand with cross-laminae (Figs. 3, 7). Along Gorst Creek, unit B1 is up to 30-cm thick and contains rip-up clasts and leaves near the base. Overlying unit B2 is up to 70-cm thick and contains structures including inclined laminae and coarser and finer layers (Fig. 3).

Charcoal from the paleosol below unit B in Otto Jarstad Park yielded an age of A.D. 570–690 (Table 2). Along Gorst Creek, the base of unit B1 contains rip-up clasts of peat and leaves (Fig. 3). Three different leaves from the lowest 5 cm of unit B1, 2.3 km upstream from Sinclair Inlet, yielded radiocarbon ages of A.D. 890–990, 720–940, and 690–880 (Fig. 3; Table 2).

Unit C

In two, close-by sites in the wetlands, the shelly-mud-peat contact is split by a pebbly sand (Fig. 7), unit C. These locations are on the southwest end of the inlet near where a small drainage enters the wetlands. The deposits are faintly laminated and contain mud intraclasts. Unit C differs from units A and B because of its high concentration of pebbles and abundant laminae.

Interpretations: Age of Coseismic Uplift and Sandy Deposits

Radiocarbon ages from above and below the sand layers place the coseismic uplift in marsh and subsequent deposition of event beds at about 1100 years ago (Table 2). This indicates the events at Gorst correlate with the time period of ruptures on multiple faults in the Puget lowland, including the Seattle and Tacoma fault zones (Sherrod *et al.*, 2004; Blakely *et al.*, 2009). Radiocarbon ages from Gorst (Table 2) indicate these events occurred between A.D. 690 and 1390 and regional correlations place the events between A.D. 900 and 930 (Atwater, 1999). The limiting maximum ages from this study at Gorst are from delicate leaves most likely torn up from the underlying soil by the debris flow. These ages cluster between A.D. 690 and 990. The leaf ages better represent the limiting maximum than other ages because the shell and charcoal were sampled centimeters below the event horizon. The shell was articulated and within 5 cm of the bottom of the sand deposit but it is unknown if the tsunami eroded any sediment in that location. The limiting minimum age comes from a *Tsuga heterophylla* (western hemlock) cone. The sample from the basal 2 cm of the woody peat contained several other cones and many needles from *T. heterophylla*. If this concentration represents the detritus of a mature tree, several decades likely passed between the uplift event and the deposition of the cone. Therefore, the age from the cone underestimates the time of the earthquake. This study correlates both the uplift and the tsunami to an earthquake on the Seattle fault zone that has a more precise age of A.D. 900–930.

Unit A: Tsunami Deposit

Unit A has many sedimentary characteristics typical of tsunami deposition (Martin and Bourgeois, 2012). While no single characteristic defines tsunami deposits, many tsunami deposits share certain characteristics (Dawson and Shi, 2000; Bourgeois, 2009). High-energy transport and grains falling out of suspension commonly dominate tsunami deposition on a coastal plain. Suspended-load sedimentation typically leads to massive, laminated, or fining-upward sandy deposits (Bourgeois, 2009). Tsunami deposits are also often described as thin (typically less than 25-cm-thick), sheetlike, thickening into depressions, and fining landward (e.g., Dawson and Shi, 2000; Tuttle *et al.*, 2004; Morton *et al.*, 2007).

Consistent with modern tsunami deposits, unit A fines upward, in this case from coarse sand and pebbles to silt

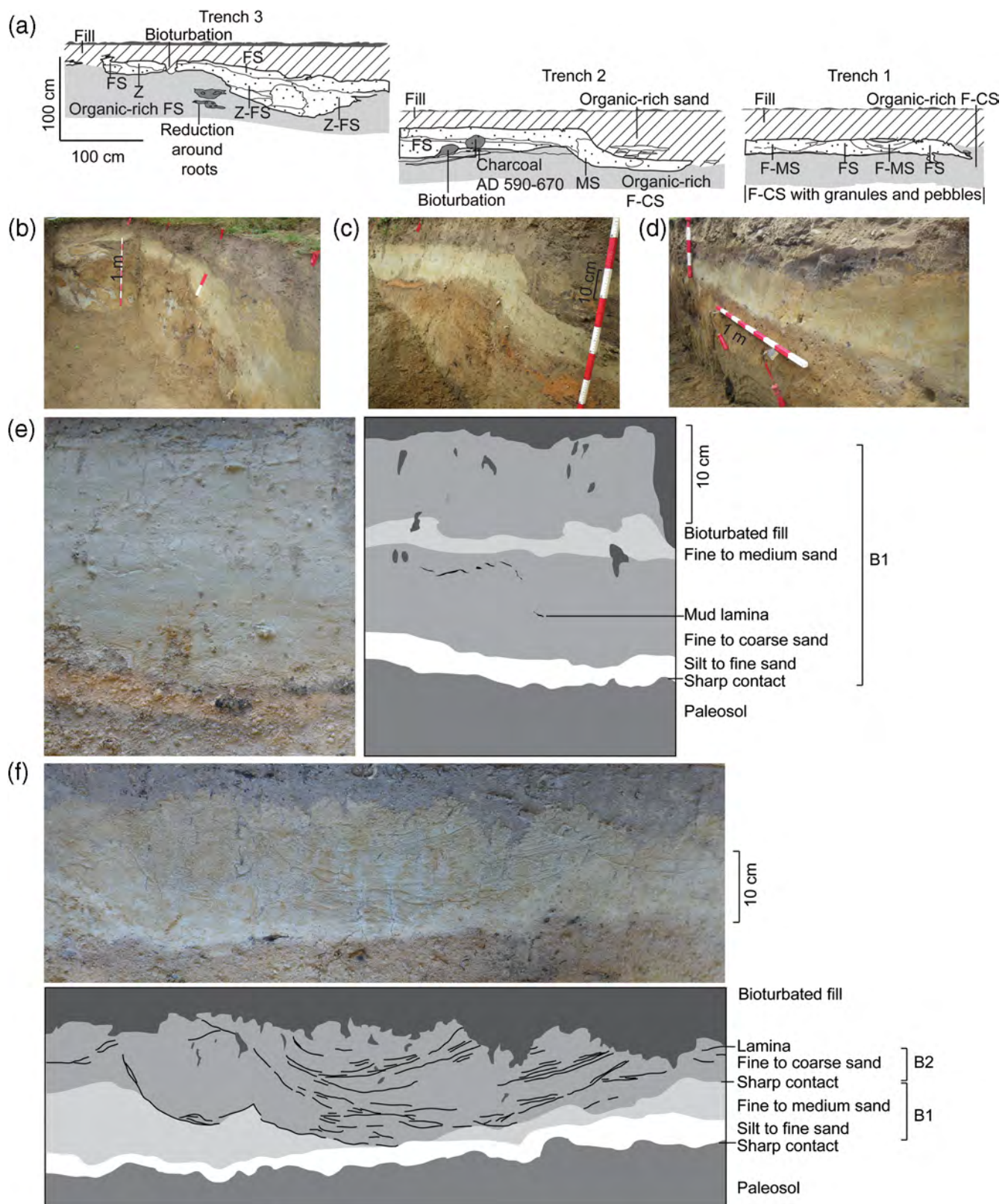


Figure 6. Unit B in Otto Jarstad Park showing massive structure of unit B1 and cut-and-fill structures in unit B2. (a) Sedimentary structures of sand unit from backhoe trenches in Otto Jarstad Park. FS, fine sand; MS, medium sand; CS, coarse sand; Z, silt. (b) Photo from of trench 3. (c) Photo of trench 2. (d) Photo of trench 1. (e) and (f) Paired photos and interpretation of sediment peels made from trench walls. (e) Trench 2. (f) Trench 1. The color version of this figure is available only in the electronic edition.

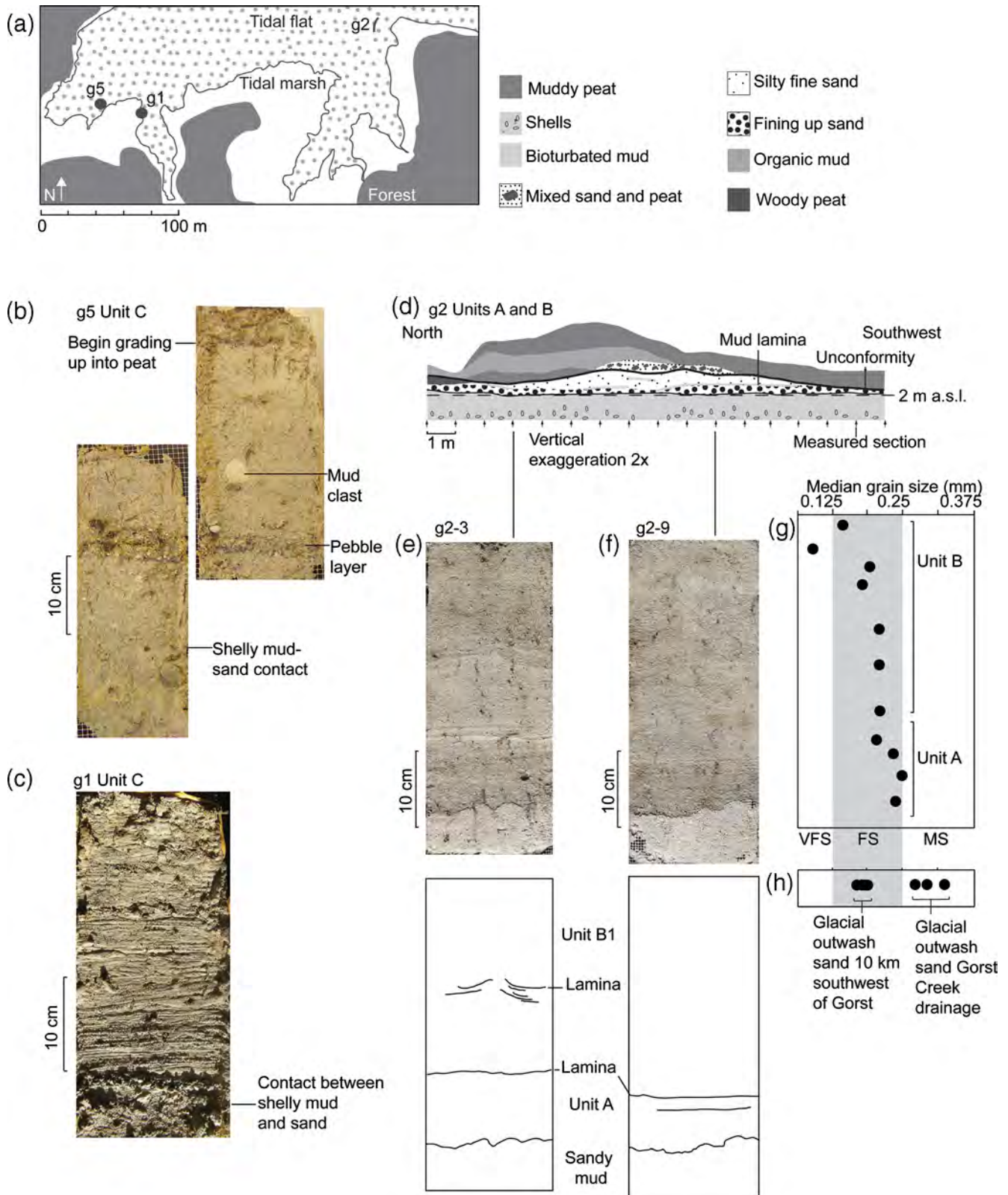


Figure 7. Peels of deposits from Gorst wetland. Unit C differs from units A and B in sedimentary structures and grain size. (a) Index map. (b) and (c) at site g5. Peels of unit C. (b) Two peels taken side by side to represent the entire deposit thickness. The pebbles in (b) and the distinct laminae in (c) are absent in (e) and (f). (d) Outcrop g2. (e) and (f) Peels from outcrop. (g) Median grain size of sedimentary units at Gorst showing fining-upward nature of both unit A and unit B. Unit B and glacial outwash sand are similar sizes. Median grain size of units A and B from the g2 outcrop in the wetlands. (h) Median grain size of glacial outwash sand from the area surrounding Gorst. The color version of this figure is available only in the electronic edition.

and fine sand. It has a sharp basal contact, a somewhat consistent thickness, and is stratigraphically associated with an apparently abrupt land-level change. The deposit is less than 25-cm-thick, sheetlike, and thickens into lower topography. The deposit disappears landward, indicating deposition from a Sinclair Inlet source, although the small geographic extent of the observed deposit limits conclusions that can be made about landward thinning and fining. Additionally, the deposit is temporally and geographically associated with an event known to have generated a tsunami (Atwater and Moore, 1992; Bourgeois and Johnson, 2001).

Interestingly, unit A is typically not found in areas where unit B is not present, especially on the northern edge of Sinclair Inlet (Fig. 5). This may be because in areas where unit B was deposited, it protected unit A from erosion and bioturbation. In sites in the wetland where I was unable to distinguish the presence of unit A, the unit B event may have eroded the underlying mud lamina and part or all of the unit A sand layer.

Alternatives to tsunami deposition include storms and liquefaction. The short fetch, lack of sedimentary structure indicating multiple waves, and absence of other similar deposits make storm deposition unlikely (Morton *et al.*, 2007). Deposition by sand blow usually results in the presence of sand dikes, spatially variable sedimentary structures, and highly variable deposit thickness (Martin and Bourgeois, 2012).

Unit B: Debris-Flow Deposit

The mapped extent and internal sedimentary structure of unit B indicate that it likely originated as a slope failure up Gorst Creek that then flowed down the creek as a sandy debris flow. Typically, debris-flow deposits are characterized by massive or inversely graded structure and the deposits coat valley floors (Pierson and Scott, 1985; Scott, 1988; Major, 1997). Debris flows are thought either to freeze or to evolve into more dilute flows. If the flow becomes more dilute through time, the resulting deposit becomes more stratified downstream and up section. The deposits from this more dilute flow can exhibit more internal sedimentary structure and fewer fines than a less dilute flow (if the original material contained clay and fine silt) (Pierson and Scott, 1985). In experimental work, Major (1997) found saturated flows typically lack internal structure, even when the deposit represented multiple debris-flow surges. In some cases, the base of a debris-flow deposit is finer than the upper portion of the deposit (inverse grading), a characteristic observed in many ancient debris-flow deposits (Vallance and Scott, 1997).

The massive structure of unit B1 and the thinning of the deposit toward the edge of the valley are consistent with deposition by debris flow. Rip-up clasts of mud and peat in the deposit also indicate a high-shear flow. However, cut-and-fill structures and lamination in the upper portion of the deposit (unit B2) indicate the debris flow either became less concentrated through time or a braided stream formed in response to the increased sediment load in Gorst

Creek. Braided stream channel processes are evident from the cross-laminae and cut-and-fill structures present in unit B2 (Fig. 6).

The presence of the deposit along the Gorst Creek valley bottom but not along tributaries indicates the origin of the deposit from the watershed of Gorst Creek. Thick, steep outcrops of recessional glacial outwash sands along Gorst Creek (Fig. 2) provide likely source material for the slope failure and deposit. The exposures along Gorst Creek are commonly steep and comprised of unconsolidated glacial-age materials including sand and laminated mud. If these moderately well-sorted outwash sands are the source material, it would explain why the deposit shows little variation in grain size (Fig. 7).

The massive structure of the deposit is consistent with deposition by debris flow rather than by other methods. Other potential processes include fluvial deposition that is not likely to generate massive structure liquefaction, which typically creates patchy deposits with common sedimentary structures, and landslide deposits that are not likely to be as widespread or have as consistent of a thickness. It is possible that a landslide-dam failure generated the debris flow; prehistoric landslide-dammed lakes are known from the Puget lowland (Logan *et al.*, 1998).

Unit C: Reworked Slope Failure

The pebbly unit C (Fig. 7) in the wetlands likely represents local slope failure from another sediment source possibly from up the nearby drainage. The laminae indicate that deposition in this area may have been due to a lower-concentration flow than the Gorst Creek debris flow or a flow that was later reworked. The small spatial distribution of the pebbles indicates this sediment pulse was not as large as the one that generated unit B, which blanketed majority of the wetlands.

Tsunami Simulations

Tsunami simulations provide timing of different events, likely tide level during the event, and demonstrate how different proposed fault models change the tsunami characteristics. Simulations also provide further information about the tsunami including estimates of wave height, form, and arrival time. The complex bathymetry of Puget Sound makes tsunami modeling necessary, as it is difficult to predict how waves will interact and resonate. Based on the geologic setting at Gorst, the tsunami deposit is most likely from the A.D. 900–930 Seattle-fault-zone earthquake. The earthquake is known to have generated a tsunami (Atwater and Moore, 1992; Koshimura *et al.*, 2002), and the deposit is associated with evidence for this earthquake (uplift). However, the Seattle fault is not the only known tsunami source from this time period. The Tacoma fault also likely generated a tsunami during this time period (Venturato *et al.*, 2007), and this tsunami may have been large enough to generate deposits at Gorst.

Simulation Parameters: Fault Slip and Sea Level

Tsunami simulations were used to replicate Seattle- and Tacoma-fault-zone tsunamis in Sinclair Inlet. Fault-slip parameters were based on previous regional tsunami simulation work for hazard analysis (Venturato *et al.*, 2007) and on simulations validated using the tsunami deposit at Cultus Bay (Koshimura *et al.*, 2002; Fig. 1; Table 3). Simulation runs included the Seattle and Tacoma fault scenarios as well as a simulation with higher slip on the western end of the Seattle fault, the latter in order to represent the uplift at Gorst from this study (Table 3; Fig. 8, Seattle up slip). Both the Seattle and Tacoma fault scenarios of Venturato *et al.* (2007) are based on reconstructing coseismic uplift(s) that correlate temporally with deposition of the tsunami sand sheet at Gorst. Using the parameters from Venturato *et al.* (2007), inputting both Seattle and Tacoma fault deformation to the same simulation represents the hypothesized case of the Seattle

and Tacoma fault zones rupturing simultaneously (Johnson *et al.*, 2004; Sherrod *et al.*, 2004; Fig. 8f, Seattle–Tacoma).

Simulations at various grid resolutions (Fig. 8b) tested the ability of grid resolution to accurately simulate the tsunami waves in Puget Sound. Other studies have shown that better grid resolution typically increases wave height, although the waveform begins to converge at increasingly higher resolutions (Titov and Synolakis, 1997; Pan *et al.*, 2010). Simulations at three resolutions show convergence of the waveform of the first, highest wave but divergence on later waves. Due to interest in only the maximum wave height, convergence demonstrates the grid resolution of the bathymetric grid was refined enough to accurately simulate the tsunami waves in Puget Sound.

Sea level varied in different simulations because the sea level at the time of the earthquake is unknown. Most simulations were run with the water at NAVD88 0, though several

Table 3
Fault Parameters from Tsunami Models

Fault Segment*	Length (km)	Width (km)	Dip	Rake	Strike	Depth (km) [†]	Slip (m)
Seattle NOAA [‡]							
S1	15.2	35	60	90	87.9	0.5	1
S2	6.3	35	60	90	86.6	0.5	1
S3	8.9	35	60	90	96	0.5	12
S4	2	35	60	90	99.3	0.5	11
S5	11.5	35	60	90	99.3	0.5	4
S6	14.9	35	60	90	81	0.5	1
Seattle Koshimura [§]							
K1	15.2	6	60	90	87.9	0.5	4
K2	6.3	6	60	90	86.6	0.5	6
K3	8.9	6	60	90	96	0.5	8
K4	2	6	60	90	128.8	0.5	8
K5	11.5	6	60	90	99.3	0.5	6
K6	14.9	6	60	90	81	0.5	4
K7	15.2	38	25	90	87.9	5.5	2
K8	6.3	38	25	90	86.6	5.5	4
K9	8.9	38	25	90	96	5.5	6
K10	2	38	25	90	128.8	5.5	6
K11	11.5	38	25	90	99.3	5.5	4
K12	14.9	38	25	90	81	5.5	2
Tacoma NOAA [‡]							
T1	10	14.1	45	90	268.9	0.5	5.6
T2	10	14.1	45	90	260.812	0.5	4
T3	10	14.1	45	90	274.046	0.5	8
T4	8	14.1	45	90	276.274	0.5	1.4
T5	8	14.1	45	90	279.473	0.5	1.4
Seattle Up Slip							
U1	15.2	35	60	90	87.9	0.5	4
U2	6.3	35	60	90	86.6	0.5	3
U3	8.9	35	60	90	96	0.5	12
U4	2	35	60	90	99.3	0.5	11
U5	11.5	35	60	90	99.3	0.5	4
U6	14.9	35	60	90	81	0.5	1

*Fault segments are mapped on Figure 8.

[†]Depth is to the top of the fault segment.

[‡]Venturato *et al.*, 2007.

[§]Koshimura *et al.*, 2002.

^{||}Modified from Venturato *et al.*, 2007.

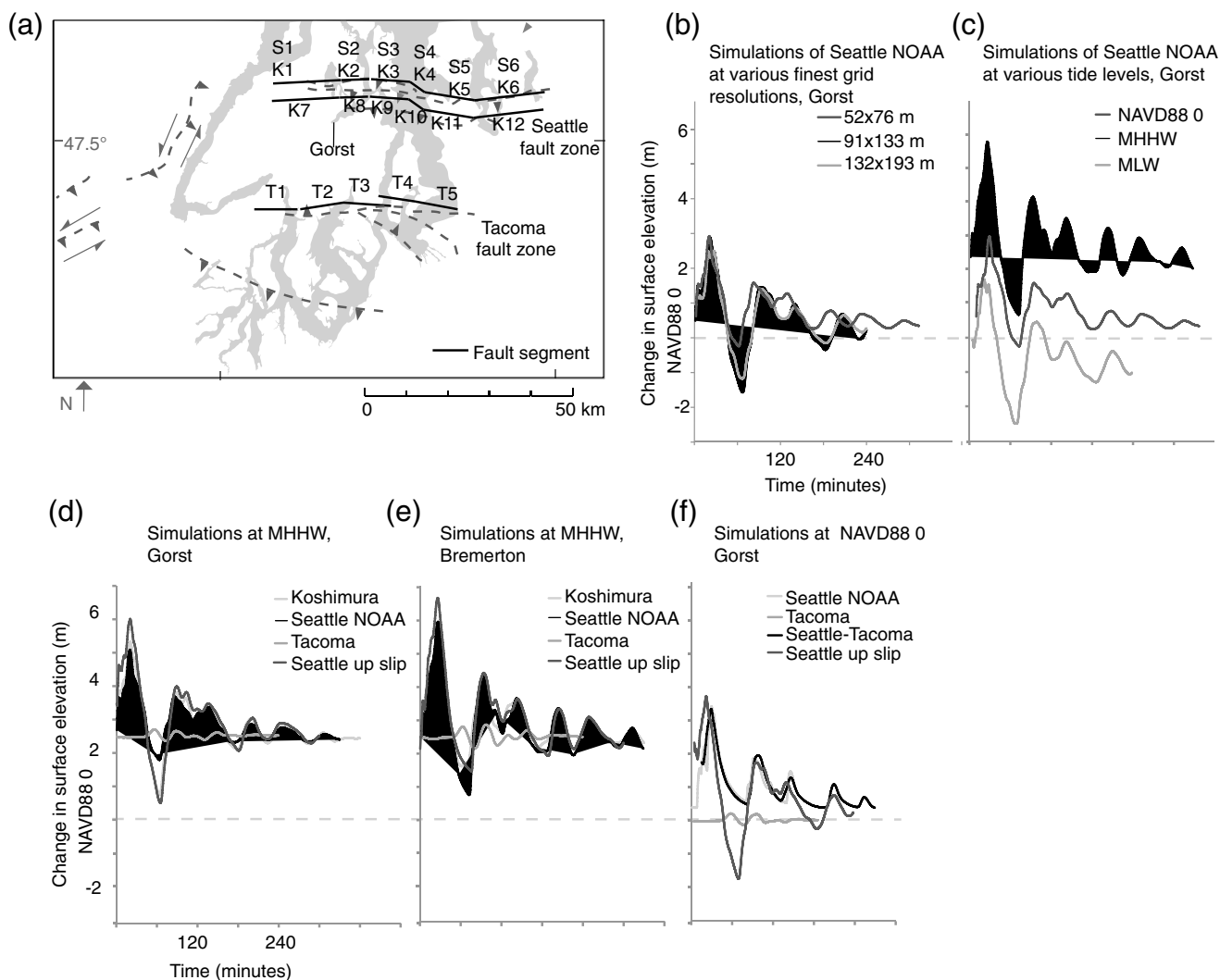


Figure 8. Simulated tide gauges from the Gorst locality for various tsunami model runs. Seattle fault simulations behave similarly and the Tacoma fault simulations are an order-of-magnitude smaller. Parameters for model runs are in Table 3. Seattle-Tacoma simulation made rupturing Seattle NOAA and Tacoma NOAA at the same time. (a) map of the top of fault segments used for simulations. Gorst tide gauge for all figures but (e) located at $N47.531^{\circ}$, -122.685° (Fig. 4a). Bremerton tide gauge for (e) at $N47.5416^{\circ}$, -122.6685° (Fig. 1). MHHW is 2.5 m higher water level than NAVD88 0. (f) MLW is 1 m below NAVD88 0.

simulations were at approximately modern mean higher high water (MHHW) (+2.5 m) and at mean low water (MLW) (−1 m; Fig. 8c). Previous modeling of the A.D. 900–930 Seattle-fault-zone tsunami (Koshimura *et al.*, 2002) set the sea level to −1 m, due to approximately 1 m of submergence of the Puget lowland in the last thousand years (Eronen *et al.*, 1987). Koshimura *et al.* (2002) concluded that with a sea level 1-m lower than modern, the tsunami would have needed to occur at high tide to explain the deposits at Cultus Bay (Fig. 1a). Unlike Cultus Bay, Gorst is in the zone of coseismic deformation for the Seattle fault zone. Before the Seattle-fault earthquake, sea level was relatively higher at Gorst than today. This higher sea level is demonstrated by marine shelly-mud above modern tide range at the landward end of the modern vegetation profile (Fig. 4). Therefore, because setting one sea level on modern bathymetry

does not represent the sea level before the earthquake, simulations at various sea levels examined the error in tsunami wave height from variability in paleo-sea level (Fig. 8c).

All tsunami simulations based on the Seattle fault zone produced wave heights of 4.0–5.5 m at Gorst, and simulations based on the Tacoma fault produced significantly lower wave heights (0.2–0.5 m; Fig. 8). For all Seattle fault-zone simulations the first wave is the largest of the tsunami wave train, with the wave reaching Gorst almost immediately after the earthquake, and the peak amplitude arriving in less than 20 minutes. The largest wave in both Gorst and Bremerton is from the simulation with increased slip at the western end of the fault (Seattle up slip). The simulated wave heights at Bremerton (Fig. 8e) are consistently higher than at Gorst (Fig. 8d), indicating the wave loses energy as it flows through Sinclair Inlet. For Tacoma fault-zone models, the

second wave is the largest, and the first wave arrives after about 30 minutes, with the peak of the first wave at approximately 40 minutes. Simulating the Seattle and Tacoma faults rupturing at the same time did not increase the maximum wave height at Gorst, but it did increase the height of later waves in the tsunami wave train (Fig. 8c, Seattle–Tacoma).

Interpretation

It is more likely that the Seattle fault zone generated the tsunami-deposited sand layer at Gorst. The Tacoma-fault-zone scenario produced no more than a 0.5-m wave height at Gorst. It is unlikely a half-meter wave could produce the up to 20-cm-thick deposit that is found in the wetlands, so the unit A deposit is more likely from a Seattle-fault-zone tsunami. Because both faults rupturing at the same time did not change the wave pattern (Fig. 8f, Seattle–Tacoma), the Seattle and Tacoma faults rupturing at the same time could also have generated the deposit at Gorst.

The tide stage at the time of the earthquake is unknown. However, due to the 3.58-m spring-tide range and uncertainties in the relative sea level at the time of the tsunami, the simulations were run at various sea levels. The results of these simulations show a 57-cm difference in wave amplitude (above respective tide levels) between MHHW and MLW simulations (Fig. 8c). When added to the difference in water elevation, this is more than a 4-m difference in flow depth. The tsunami deposits at Gorst are currently approximately 2 m above NAVD88 0 (Fig. 5). The simulated MLW (1 m below NAVD88 0) tsunami does not reach this elevation; therefore, water level at the time of the earthquake was higher than mean lower low water (MLLW).

Timing of Uplift, Tsunami, and Debris Flow

Stratigraphy and regional correlations indicate minutes to months between the tsunami and debris flow. Flame structures within the capping mud of the tsunami deposit indicate this mud was still saturated when the debris flow covered the mud lamina, but the fine grains that form the lamina had time to settle out of suspension. Unit A likely was deposited by the first tsunami wave because it was the largest wave based on simulations. The earliest event the mud may represent is the lull that occurred after the first wave, approximately one hour after the earthquake (Fig. 8). Persistent saturation is more likely for a winter, rainy-season event, which is consistent with analysis of tree rings indicating the Seattle-fault earthquake occurred between the growing seasons of trees (Jacoby *et al.*, 1992). Further constraints on timing include a lack of evidence of vegetation or soil formation on top of the lamina before burial by the debris flow. The flame structures further indicate the lack of stabilizing vegetation. The presence of stabilizing roots and baffling stems would prevent the deformation of the mud into flames. Given coseismic uplift into a forest zone, this lack of weathering or soil indicates vegetation did not grow on the surface before the

debris-flow sands coated the area. Depending on the rate of colonization, this period may span a few years.

If, as is likely, the debris flow initiated during earthquake shaking, the tsunami and debris flow may have interacted, but the preservation of two distinct deposits in the wetlands do not support this interaction. Estimations of debris-flow speed indicate that the debris flow initiated some time after the earthquake or that the debris flow had a low velocity. Debris-flow speed is dependent on slope, concentration, and grain size of the flow (Iverson, 1997), and flow velocities for debris flows range between 36 m/s and 1.8–2.0 m/s (Davies *et al.*, 1992; Iverson, 1997; Genevois *et al.*, 2001). Therefore, the rate the Gorst debris flow would have traveled the 2 km from farthest mapped deposit in approximately 1 minute to 15–20 minutes. However, it is likely that the debris flow initiated at some point farther upstream. The headwaters of Gorst Creek are approximately 4 km from the wetlands, and if the debris flow initiated there the slow debris flow would take 30–40 minutes to reach the wetlands.

Given the evidence and arguments that the debris flow was delayed long enough to allow a mud lamina to be preserved on top of the deposit of the tsunami's first wave, but short enough that there is no evidence of a passing season between the tsunami and debris flow, there remain several explanations for the stratigraphic order. (1) The debris flow was slowed by the gentle slope of Gorst Creek and the old-growth forest. (2) The debris flow was triggered by an earthquake on another fault or by an aftershock. (3) The slope failure occurred hours to days after the earthquake, although seismically generated landslides typically fail during the earthquake, in some cases, such as the 1949 Tacoma Narrows slide (Chleborad, 1994), slides occur days after the earthquake. (4) A landslide-dammed lake formed and later failed catastrophically (as in Capart *et al.*, 2009).

Discussion and Conclusions

Stratigraphic relationships between the deposits and thus the associated events indicate uplift, shortly followed by a tsunami, followed by a debris flow up from Gorst Creek (Fig. 9). The close stratigraphic association of the uplifted paleo-surface with an overlying tsunami deposit is best explained if the uplift was coseismic and the tsunami produced by the same regional coseismic deformation.

A.D. 900–930 Seattle-Fault Earthquake Deformation

This study indicates coseismic deformation farther south and with higher uplift during the A.D. 900–930 Seattle-fault-zone rupture than previous fault interpretations (e.g., ten Brink *et al.*, 2006; Kelsey *et al.*, 2008), and this uplift may have implications for the fault structure. Further, the distribution and height of the marine terraces from the A.D. 900–930 earthquake is used to corroborate fault models. Therefore, revised deformation width and height may change

the possible interpretations of the structure of the Seattle fault zone. A minimum of 3 m of uplift at Gorst, as found in this study, is double the uplift estimated by previous fault models for the location (Koshimura *et al.*, 2002; ten Brink *et al.*, 2006; Fig. 10). This work indicates that the zone of deformation of the Seattle fault may not be as narrow as estimated by the presence of marine terraces by giving evidence of uplift 3 km west and 1.5 km south of the farthest extent of mapped terraces. South of Seattle, 3-m-high marine terraces are traced approximately the same distance south of the Seattle fault as Gorst (ten Brink *et al.*, 2006), indicating a broader zone of deformation along the length of the A.D. 900–930 rupture. A broader zone of deformation may indicate either a wider zone of slip along the dip of the fault, a shallower dip, or splay faults farther to the south. An anticline in the bedrock north of Gorst (Fig. 1c) might also have been the origin of higher than expected uplift in Gorst. It is unclear if the anticline is an active or relict structure.

Because Gorst's at least 1.5 m of submergence in the last thousand years cannot be explained as local compaction of sediments (which is unlikely due to shallow bedrock), more uplift occurred along the Seattle fault in A.D. 900–930 than has been estimated previously. Widespread submergence would indicate that marine terraces formed in that event were originally at least 1.5 m higher above sea level than they are at present. This would increase the terrace height by 14%–90% (Fig. 10). If so, refined values of terrace heights, including the additional 1.5 m, may have an impact on reconstructions of fault geometry and slip. Moreover, the 1.5 m of submergence in the 1100 years since the earthquake may have obscured the uplift record in areas with only a meter or two of coseismic uplift as these lower terraces would now be within the tidal range. Therefore, higher uplift also supports this study's other conclusion that the band of deformation from the A.D. 900–930 earthquake was broader than previously modeled.

Timing and Causes of Postseismic Submergence

Return of a coseismically uplifted, forested area to intertidal conditions occurred some time between A.D. 1520 and 1880 in portions of the wetlands. These ages are based on an *in-situ Thuja plicata* snag in what is now the salt marsh and on the earliest maps of the region. Based on radiocarbon dating, this snag died sometime after the period of A.D. 1520 and 1660 (C. Garrison-Laney, unpublished data). The earliest U.S. Coastal Survey map of the Gorst area shows the salt marsh at approximately its current extent (Ellicott, 1881). Therefore, the return to intertidal conditions occurred sometime between when the tree was alive (A.D. 1520 and 1660) and when the area was first mapped (A.D. 1880). These ages and the stratigraphy do not indicate if there was a rapid submergence event after A.D. 1520 or if slow submergence returned the forest to the intertidal zone after this time.

Peat records from other areas in the region indicate little sea level variation in the time period of interest and a regional

signal of submergence. Clague *et al.* (1982) and Williams and Roberts (1989) found little to no sea level variation in the last 1500 years in southern British Columbia indicating that the submergence in Gorst is not due to eustatic or regional sea level rise. Peat records from north of Gorst in the Puget lowland indicate <1 m of relative sea level rise in the last thousand years (Eronen *et al.*, 1987; Beale, 1990). Sherrod *et al.* (2000)'s work on Restoration Point (Fig. 1b) has an obscured post-A.D. 900–930 earthquake record but does show an early event of submergence at ~A.D. 250. They link this record to tectonic submergence but do not infer a source. These records indicate that the southern Puget lowland may be subsiding at a higher rate than the northern Puget lowland and British Columbia.

The source of the postearthquake submergence is not well understood but is likely due to processes related to the subduction zone. There are two hypotheses as to why the sites in the Puget lowland are subsiding. First, forearc basins commonly subside. Reasons for forearc basin subsidence include underplating by the accretionary prism, growth, and widening of the basin (Xie and Heller, 2009). Second, Garrison-Laney (2003) hypothesized submergence at Gorst and other sites in the Puget lowland may be linked to the rapid submergence during the A.D. 1700 Cascadia subduction zone earthquake.

Evidence of submergence is most likely the result of gradual forearc submergence. Widespread evidence of submergence in the last 1100 years (Bucknam *et al.*, 1992; Sherrod, 2001; Martin, 2011) of more than a meter in some locations indicates slip on the subduction zone is a less likely candidate because subsidence farther away from the subduction zone should be less than subsidence near the subduction zone. Subsidence on the western coast of Oregon during the A.D. 1700 earthquake was typically less than a meter (Hawkes *et al.*, 2011). It is unexpected that subsidence would be 50% higher farther away from the plate boundary. Further, it is unlikely that the submergence is due to shallow crustal faults in the Puget lowland. Sites with records of submergence are adjacent to different crustal faults zones including the Seattle, Tacoma, and Saddle Mountain (this study; Sherrod *et al.*, 2004; Martin, 2011). The sites experiencing submergence are varying distances from faults and have different histories of coseismic land-level change, yet they all show over a meter of submergence. It is unlikely that all areas would show similar submergence if the mechanism is related to crustal faulting. Better stratigraphic control on sea level change through paleoenvironmental methods and dating would help to clarify the rate and timing of submergence.

Implications for Hazard Planning

This study reiterates the threat of multiple hazards associated with earthquakes in the Puget lowland, of which tsunamis are prominent in the case of Sinclair Inlet. Tsunami deposits at Gorst and tsunami modeling reiterate the tsunami threat in this inlet. Evidence for a tsunami in Sinclair Inlet is

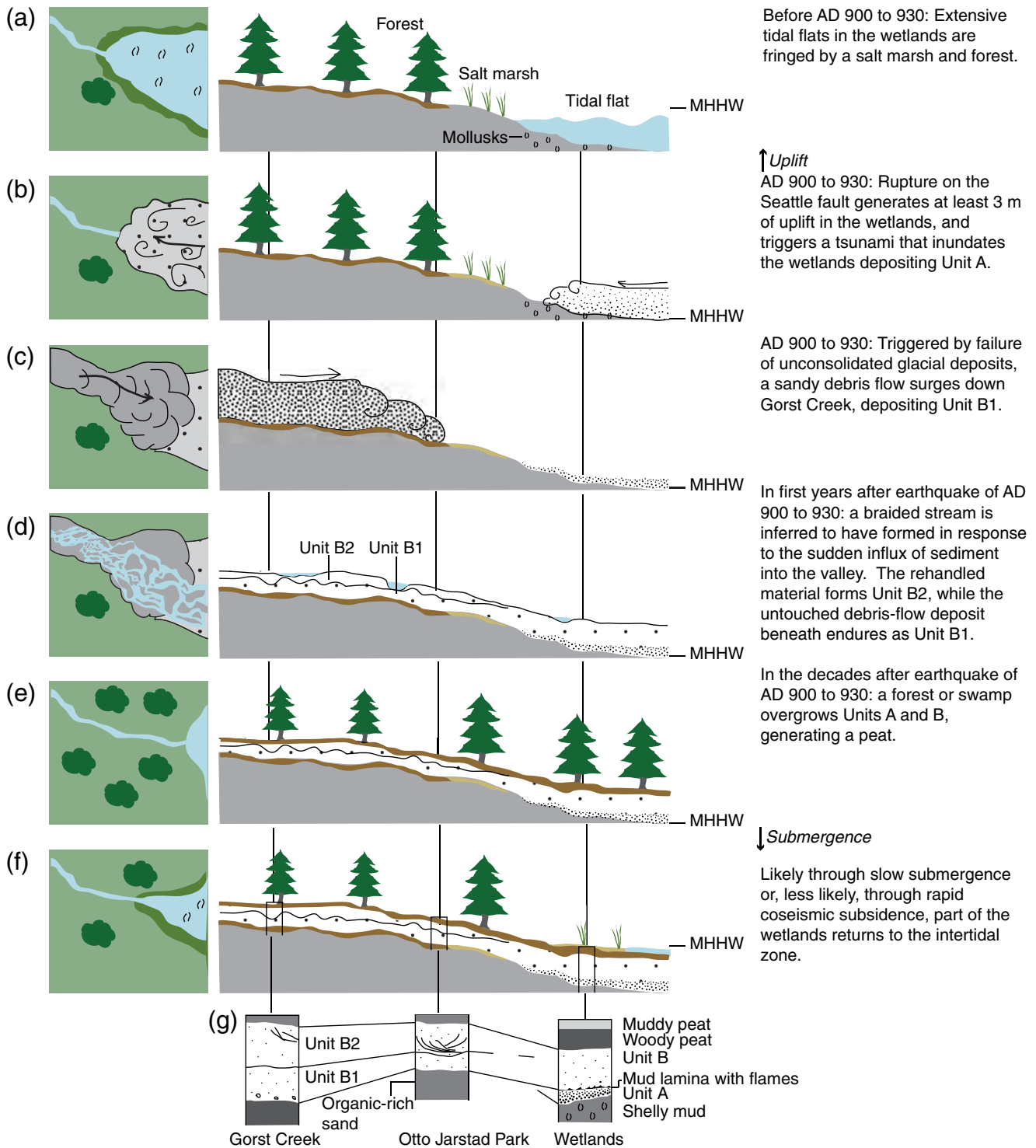


Figure 9. Cartoon of main geological events recorded at Gorst including relative changes in mean higher high water (MHHW). Map view in the left column schematic cross-section in the right column. (a) Pre-earthquake conditions. (b) Tsunami and deposition of unit A. (c) Debris flow and deposition of unit B. (d) Reworking of unit B by braided stream flow. (e) Establishment of forest and swamp after the earthquake. (f) Modern conditions. (g) Generalized stratigraphic sections from Gorst placed below the location in the cross-section the stratigraphy represents. The color version of this figure is available only in the electronic edition.

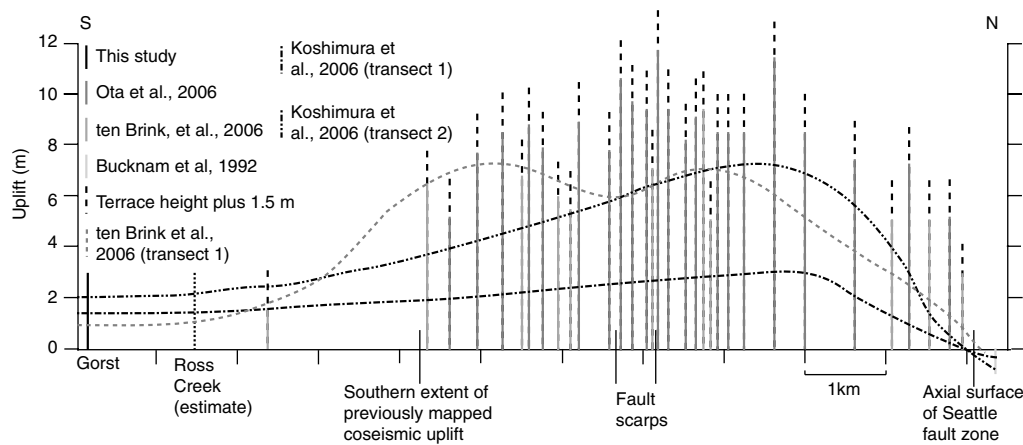


Figure 10. Terrace heights projected onto a north–south transect across the Seattle fault zone showing a reconstruction of initial terrace height factoring in 1.5 m of submergence from transect 2 in Figure 1. Uplift values from the A.D. 900–930 from marine terrace heights and marsh stratigraphy are projected onto the transect. *ten Brink et al. (2006)* estimate error in their terrace data to be ± 1 m. *Ota et al. (2006)* estimate the error on terrace heights to be at least the ± 30 cm error of the LiDAR data used to measure terrace heights. The highest terrace heights on Bainbridge Island are likely the result of two coseismic uplift events (*Kelsey et al., 2008*). Dashed lines represent original terrace heights accounting for 1.5 m of submergence. Modeled deformation from different fault geometries along transects 1 and 2 on Figure 1 from *ten Brink et al. (2006)* and *Koshimura et al. (2002)*.

not unexpected based on the proximity to the Seattle fault zone and on previous tsunami models (*Koshimura et al., 2002*). Simulated wave heights of 4–5 m indicate tsunamis are not only a threat to the infrastructure in Gorst, but also to the naval base at Bremerton. Tsunami simulations demonstrate that the higher uplift documented in this study results in almost a meter higher tsunami wave along Sinclair Inlet. Even an order-of-magnitude smaller Tacoma fault-generated tsunami would generate strong currents in the narrow straits and harbors near Gorst. Further tsunami simulations in the Puget lowland including different fault scenarios would help determine the degree of hazard posed by locally generated tsunamis.

Understanding background submergence rates is important for planning for future sea level rise. A rate of submergence of 1.5 m per 1100 years is higher than predicted for the Gorst region (*Reilinger and Adams, 1982; Holdahl et al. 1989; Shipman, 1989; Mitchell et al. 1994; Hyndman and Wang, 1995*). Currently, the long-term rate of submergence and the variability in this rate across the Puget lowland are constrained by only a few data points. Further studies and detailed dating would help to bracket the rate of submergence and produce better input for models of sea level rise.

Data and Resources

The t-sheet (*Ellicott, 1881*) is published and accessed through the Puget Sound River History Project at <http://riverhistory.ess.washington.edu/tsheets> (last accessed December 2010). The tsunami model (GeoCLaw) is an open source code available at <http://www.amath.washington.edu/~dgeorge/tsunamimodeling.html> (last accessed Month Year). The bathymetry and topography (*Finlayson, 2005*) used for tsunami modeling is available at <http://www.ocean.washington>

[.edu/data/pugetsound/](http://data.pugetsound/) (last accessed October 2010). Radiocarbon dates calibrated using OxCal are available at <https://c14.arch.ox.ac.uk/oxcal/> (last accessed March 2011).

Acknowledgments

This project was funded by USGS-NEHRP Award *07HQGR0009* and an ExxonMobil student grant, as well as fellowship assistance from the University of Washington Department of Earth & Space Sciences. Thank you to B. Atwater for identifying the site and giving me invaluable advice. D. Sullivan aided with the grain-size analysis. E. Nesbitt of the Burke Museum aided in identifying shells. K. Mandli and R. LeVeque were invaluable in describing the use of GeoCLaw. This study benefitted greatly from comments from B. Atwater, J. Bourgeois, C. Nittrouer, B. MacInnes, and S. P. La Selle and reviews by H. Kelsey and K. Clark. Many thanks to numerous agencies and landowners who permitted access, especially the City of Bremerton Department of Public Works.

References

- Atwater, B. F. (1999). Radiocarbon dating of a Seattle earthquake to A.D. 900–930, *Seismol. Res. Lett.* **70**, 232.
- Atwater, B. F., and A. L. Moore (1992). A tsunami about 1000 years ago in Puget Sound, *Wash. Univ. Stud. New Sci. Tech.* **258**, 1614–1617.
- Barnhardt, W. A., and B. L. Sherrod (2006). Evolution of a Holocene delta driven by episodic sediment delivery and coseismic deformation, Puget Sound, Washington, USA, *Sedimentology* **53**, 1211–1228.
- Beale, H. (1990). Relative rise in sea-level during the past 5000 years at six salt marshes in northern Puget Sound, Washington, *Shorelines and Coastal Zone Management Program*, Washington Department of Ecology, Olympia, Washington, 55 pp.
- Berger, M. J., D. L. George, R. J. LeVeque, and K. T. Mandli (2011). The GeoCLaw software for depth-averaged flows with adaptive refinement, *Adv. Water Resour.* **34**, 1195–1206.
- Blakely, R. J., R. E. Wells, C. S. Weaver, and S. Y. Johnson (2002). Location, structure, and seismicity of the Seattle fault zone, Washington: Evidence from aeromagnetic anomalies, geologic mapping, and seismic-reflection data, *Geol. Soc. Am. Bull.* **114**, 169–177.

- Blakely, R., B. L. Sherrod, J. F. Hughes, M. L. Anderson, R. E. Wells, and C. S. Weaver (2009). Saddle Mountain fault deformation zone, Olympic Peninsula, Washington: Western boundary of the Seattle uplift, *Geosphere* **5**, 105–125.
- Booth, D. B. (1994). Glaciofluvial infilling and scour of the Puget lowland, Washington, during ice-sheet glaciation, *Geology* **22**, 695–698.
- Bourgeois, J. (2009). Geologic effects and records of tsunamis, in *The Sea*, A. Robinson and E. Bernard (Editors), Vol. **15**, Harvard University Press, Cambridge, Massachusetts, 55–91.
- Bourgeois, J., and S. Y. Johnson (2001). Geologic evidence of earthquakes at the Snohomish delta, Washington, in the past 1200 yr, *Geol. Soc. Am. Bull.* **113**, 482–494.
- Brocher, T. M., R. J. Blakely, and R. E. Wells (2004). Reinterpretation of the Seattle uplift, Washington, as a passive roof duplex, *Bull. Seismol. Soc. Am.* **94**, 1379–1401.
- Bucknam, R. C., E. Hemphill-Haley, and E. B. Leopold (1992). Abrupt uplift within the past 1700 years at southern Puget Sound, Washington, *Science* **258**, 1611–1614.
- Capart, H., D. L. Young, and Y. Zech (2009). Dam-break induced debris flow, in *Particulate Gravity Currents* W. McCaffrey, B. Kneller, and J. Peakall (Editors), Vol. **14**, Blackwell Publishing Ltd., Oxford, 9–158.
- Chleborad, A. F. (1994). Modeling and analysis of the 1949 Narrows Landslide, Tacoma, Washington, *Bull. Assoc. Eng. Geol.* **3**, 305–327.
- Clague, J. J., J. R. Harper, R. J. Hebda, and D. E. Howes (1982). Late Quaternary sea level and crustal movements, coastal British Columbia, *Can. J. Earth Sci.* **19**, 597–618.
- Davies, T. R., C. J. Phillips, A. J. Pearce, and X. B. Zhang (1992). Debris flow behavior—An integrated overview, *Proc. Chengdu Symp.* **209**, 217–227.
- Dawson, A. G., and S. Shi (2000). Tsunami deposits, *Pure Appl. Geophys.* **157**, 875–897.
- Dragovich, J. D., P. T. Pringle, and T. J. Walsh (1994). Extent and geometry of the mid-Holocene Osceola mudflow in the Puget lowland—Implications for Holocene sedimentation and paleogeography, *Wash. Geol.* **22**, 3–26.
- Deo, J. N., J. Stone, and J. Stein (2004). Building confidence in shell: Variations in the marine radiocarbon reservoir correction for the northwest coast over the past 3,000 years, *Am. Antiq.* **69**, 771–786.
- Ellicott, E. (1881). Shore topography of Port Orchard, Puget Sound, Washington territory, *U.S. Coast and Geodetic Survey*, access through the Puget Sound River History Project, <http://riverhistory.ess.washington.edu/tsheets> (last accessed December 2010).
- Eronen, M., T. Kankainen, and M. Tsukada (1987). Late Holocene sea-level record in a core from the Puget lowland, Washington, *Quaternary Res.* **27**, 147–159.
- Finlayson, D. P. (2005). *Combined bathymetry and topography of the Puget lowland, Washington State*, University of Washington Press, Seattle, Washington.
- Garrison-Laney, C. (2003). Subsidence within the last 600 years at Puget Sound, Washington, *Abstr. Programs Geol. Soc. Am.* **35**, 582.
- Genevois, R., A. Galgaro, and P. R. Teccs (2001). Image analysis for debris flow properties estimation, *Phys. Chem. Earth* **26**, 623–631.
- Gower, H. D., J. C. Yount, and R. S. Crosson (1985). Seismotectonic map of the Puget Sound region, Washington, *U.S. Geol. Surv. Map I-1613*.
- Hawkes, A. D., B. P. Horton, A. R. Nelson, C. H. Vane, and Y. Sawai (2011). Coastal subsidence in Oregon, USA, during the giant Cascadia earthquake of A.D. 1700, *Quaternary Sci. Rev.* **30**, 364–376.
- Haessler, P. J., and K. P. Clark (2000). Geologic map of the Wildcat Lake 7.5' Quadrangle Kitsap and Mason counties, Washington, *U.S. Geol. Surv. Open-File Rept. 00-356*.
- Haugerud, R. A. (2009). Preliminary geomorphic map of the Kitsap Peninsula, Washington, *U.S. Geol. Surv. Open-File Rept. 2009-1033*.
- Holdahl, S. R., F. Faucher, and H. Dragert (1989). Contemporary vertical crustal motion in the Pacific Northwest, in *Slow Deformation and Transmission of Stress in the Earth*, S. Cohen and P. Vanicek (Editors), American Geophysical Monograph **49**, 17–29.
- Hyndman, R. D., and K. Wang (1995). The rupture zone of Cascadia great earthquakes from current deformation and the thermal regime, *J. Geophys. Res.* **100**, 133–154.
- Iverson, R. M. (1997). The physics of debris flows, *Rev. Geophys.* **35**, 245–296.
- Jacoby, G. C., P. L. Williams, and B. M. Buckley (1992). Tree ring correlation between prehistoric landslides and abrupt tectonic events in Seattle, Washington, *Science* **258**, 1621–1623.
- James, T. S., J. J. Clague, K. Wang, and I. Hutchinson (2000). Postglacial rebound at the northern Cascadia subduction zone, *Quaternary Sci. Rev.* **19**, 1527–1541.
- James, T. S., E. J. Gowan, I. Hutchinson, J. J. Clague, J. V. Barrie, and K. W. Conway (2009). Sea-level change and paleogeographic reconstructions, southern Vancouver Island, British Columbia, Canada, *Quaternary Sci. Rev.* **28**, 1200–1216.
- Johnson, S. Y., S. V. Dadisman, J. R. Childs, and W. D. Stanley (1999). Active tectonics of the Seattle Fault and central Puget Sound, Washington: Implications for earthquake hazards, *Geol. Soc. Am. Bull.* **111**, 1042–1053.
- Johnson, S. Y., R. J. Blakely, W. J. Stephenson, S. V. Dadisman, and M. A. Fisher (2004). Active shortening in the Cascadia forearc and implications for seismic hazards of the Puget lowland, *Tectonics* **23**, TC1011.
- Karlin, R. E., and S. E. B. Abella (1992). Paleoseismicity in the Puget Sound region recorded in sediments from Lake Washington, U.S.A., *Science* **258**, 1617–1620.
- Karel, P., and L. M. Liberty (2008). The western extension of the Seattle fault: New insights from seismic reflection data, *Eos Trans. AGU* **89**, T21B–1951.
- Kelsey, H. M., B. L. Sherrod, A. R. Nelson, and T. M. Brocher (2008). Earthquakes generated from bedding plane-parallel reverse faults above an active wedge thrust, Seattle fault zone, *Geol. Soc. Am. Bull.* **120**, 1581–1597.
- Koshimura, S., H. O. Mofjeld, F. I. González, and A. L. Moore (2002). Modeling the 1100 bp paleotsunami in Puget Sound, Washington, *Geophys. Res. Lett.* **29**, 1948.
- Kozloff, E. (1983). *Seashore Life of the Northern Pacific Coast: An Illustrated Guide to Northern California, Oregon, Washington & British Columbia*, University of Washington Press, Seattle, Washington, 370 pp.
- LeVeque, R. J., and D. L. George (2008). High-resolution finite volume methods for the shallow water equations with bathymetry and dry-states, in *Advanced Numerical Models for Simulating Tsunami Waves and Runup*, Liu, P. L., C. Synolakis, and H. Yeh (Editors), **10**, World Scientific, Singapore, 43–73.
- LeVeque, R. L., D. L. George, and M. J. Berger (2011). Tsunami modeling with adaptively refined finite volume methods, *Acta Numerica* **20**, 211–289.
- Liberty, L. M., and T. L. Pratt (2008). Structure of the eastern Seattle fault zone, Washington State: New insights from seismic reflection data, *Bull. Seismol. Soc. Am.* **98**, 1681–1695.
- Logan, R. L., R. L. Schuster, P. Pringle, T. Walsh, and S. P. Palmer (1998). Radiocarbon ages of probable coseismic features from the Olympic Peninsula and Lake Sammamish, Washington, *Wash. Geol.* **26**, 59–67.
- Ludwin, R. S., C. S. Weaver, and R. S. Crosson (1991). Seismicity of Washington and Oregon, in *Neotectonics of North America*, D. Slemmons, E. Engdahl, D. Blackwell, and D. Schwartz (Editors), Geol. Soc. Am., Boulder, Colorado, 77–98.
- Major, J. J. (1997). Depositional processes in large-scale debris-flow experiments, *J. Geol.* **105**, 345–366.
- Martin, M. E. (2011). Coastal marsh stratigraphy as an indicator of past earthquakes, Puget lowland, Washington State, *Ph.D. Thesis*, University of Washington, Seattle, Washington, 186 pp.
- Martin, M. E., and J. Bourgeois (2012). Vented sediments and tsunami deposits in the Puget lowland, Washington—Differentiating sedimentary processes, *Sedimentology* **59**, 419–444.

- Mitchell, C. E., P. Vincent, R. J. Weldon, and M. A. Richards (1994). Present-day vertical deformation of the Cascadia margin, Pacific Northwest, United States, *J. Geophys. Res.* **99**, 257–278.
- Mofjeld, H. O., A. J. Venturato, V. V. Titov, F. I. Gonzalez, and J. C. Newman (2002). Tidal datum distributions in Puget Sound, Washington, based on a tidal model, *NOAA Tech. Memo. OAR PMEL-122*, 35 pp.
- Morton, R. A., G. Gelfenbaum, and B. E. Jaffe (2007). Physical criteria for distinguishing sandy tsunami and storm deposits using modern examples, *Sediment. Geol.* **200**, 184–207.
- Nelson, A. R., S. Y. Johnson, H. M. Kelsey, R. E. Wells, B. L. Sherrod, S. K. Pezzopane, L. Bradley, R. D. Koehler, and R. C. Bucknam (2003). Late Holocene earthquakes on the Toe Jam Hill fault, Seattle fault zone, Bainbridge Island, Washington, *Geol. Soc. Am. Bull.* **115**, 1368–1403.
- Okada, R. (1985). Surface deformation due to shear and tensile faults in a half-space, *Bull. Seismol. Soc. Am.* **75**, 1135–1154.
- Ota, Y., S. Odagiri, H. Sasaki, and S. Mukoyama (2006). Late Holocene deformation as deduced from the former shoreline height of marine terraces above the Seattle fault zone, Washington State, *Jishin* **58**, 385–399.
- Pan, W., S. Wang, and S. Cai (2010). Numerical simulations of the coastal effects of tsunami waves caused by the 1993 Hokkaido-Nansei-Oki earthquake, *Chinese J. Ocean. Limnology* **28**, 1029–1039.
- Pierson, T. C., and K. M. Scott (1985). Downstream dilution of a lahar: Transition from debris flow to hyperconcentrated streamflow, *Water Resour. Res.* **21**, 1511–1524.
- Pratt, T. L., S. Y. Johnson, C. J. Potter, W. J. Stephenson, and C. A. Finn (1997). Seismic reflection images beneath Puget Sound, western Washington State: The Puget lowland thrust sheet hypothesis, *J. Geophys. Res.* **102**, 469–489.
- Reimer, P. J., M. G. L. Baillie, E. Bard, A. Bayliss, J. W. Beck, P. G. Blackwell, C. Bronk Ramsey, C. E. Buck, G. S. Burr, R. L. Edwards, M. Friedrich, P. M. Grootes, T. P. Guilderson, I. Hajdas, T. J. Heaton, A. G. Hogg, K. A. Hughen, K. F. Kaiser, B. Kromer, F. G. McCormac, S. W. Manning, R. W. Reimer, D. A. Richards, J. R. Southon, S. Talamo, C. S. M. Turney, J. van der Plicht, and C. E. Weyhenmeyer (2009). IntCal09 and Marine09 Radiocarbon age calibration curves, 0–50,000 years cal BP, *Radiocarbon* **51**, 1111–1150.
- Reilinger, R., and J. Adams (1982). Geodetic evidence for active landward tilting of the Oregon and Washington coastal ranges, *Geophys. Res. Lett.* **9**, 401–403.
- Schuster, R. L., R. L. Logan, and P. T. Pringle (1992). Prehistoric rock avalanches in the Olympic Mountains, Washington, *Science* **258**, 1620–1621.
- Scott, K. M. (1988). Origins, behavior, and sedimentology of lahars and lahar-runout flows in the Toutle-Cowlitz River system, *U.S. Geol. Surv. Profess. Pap.* 1447-A, 1–74.
- Sherrod, B. L. (1999). Gradient analysis of diatom assemblages in a Puget Sound salt marsh—Can such assemblages be used for quantitative paleoecological reconstructions?, *Palaeogeography, Palaeoclimatology, Palaeoecology* **149**, 213–226.
- Sherrod, B. L. (2001). Evidence for earthquake-induced subsidence about 1100 yr ago in coastal marshes of southern Puget Sound, Washington, *Geol. Soc. Am. Bull.* **113**, 1299–1311.
- Sherrod, B. L. (2002). Late Quaternary surface rupture along the Seattle fault zone near Bellevue, Washington, *Eos Trans. AGU* **83**, S21C–12.
- Sherrod, B. L., R. C. Bucknam, and E. B. Leopold (2000). Holocene relative sea-level changes along the Seattle fault at Restoration Point, Washington, *Quaternary Res.* **54**, 384–393.
- Sherrod, B. L., T. M. Brocher, C. S. Weaver, R. C. Bucknam, R. J. Blakely, H. M. Kelsey, A. R. Nelson, and R. Haugerud (2004). Holocene fault scarps near Tacoma, Washington, USA, *Geology* **32**, 9–12.
- Shipman, H. (1989). Vertical land movements in coastal Washington: Implications for sea-level change, *Shorelands and Coastal Zone Management Program*, Washington Department of Ecology, Olympia, Washington, 41 pp.
- Shipman, H. (2001). Coastal landsliding on Puget Sound: A review of landslides occurring between 1996 and 1999, *Report #01-06-019*, Washington Department of Ecology, Olympia, Washington, 101 pp.
- Titov, V.V., and C. E. Synolakis (1997). Extreme inundation flows during the Hokkaido-Nansei-Oki tsunami, *Geophys. Res. Lett.* **24**, 315–318.
- ten Brink, U. S., J. Song, and R. C. Bucknam (2006). Rupture models for the A.D. 900–930 Seattle fault earthquake from uplifted shorelines, *Geology* **34**, 585–588.
- Thorson, R. M. (1989). Glacio-isostatic response of the Puget Sound area, Washington, *Geol. Soc. Am. Bull.* **101**, 1163–1174.
- Tuttle, M. P., A. Ruffman, T. Anderson, and H. Jeter (2004). Distinguishing tsunami from storm deposits in eastern North America: The 1929 Grand Banks tsunami versus the 1991 Halloween storm, *Seismol. Res. Lett.* **75**, 117–131.
- Vallance, J. W., and K. M. Scott (1997). The Osceola mudflow from Mount Rainier: Sedimentology and hazards implications of a huge clay-rich debris flow, *Geol. Soc. Am. Bull.* **109**, 143–163.
- Venturato, A., D. Arcas, V. Titov, H. Mofjeld, C. Chamberlin, and F. González (2007). Tacoma, Washington, tsunami hazard mapping project: Modeling tsunami inundation from Tacoma and Seattle fault earthquakes, *NOAA Tech. Memo. OAR PMEL-132*, 27 pp.
- Verdonck, D. (2006). Contemporary vertical crustal deformation in Cascadia, *Tectonophysics* **417**, 221–230.
- Williams, H. F. L., and M. C. Roberts (1989). Holocene sea-level change and delta growth—Fraser River delta, British Columbia, *Can. J. Earth Sci.* **26**, 1657–1666.
- Williams, H. F. L., and I. Hutchinson (2000). Stratigraphic and microfossil evidence for late Holocene tsunamis at Swantown Marsh, Whidbey Island, Washington, *Quaternary Res.* **54**, 218–227.
- Williams, H. F. L., I. Hutchinson, and A. R. Nelson (2005). Multiple sources for late-Holocene tsunamis at Discovery Bay, Washington State, U.S.A., *Holocene* **15**, 60–73.
- Xie, X., and P. L. Heller (2009). Plate tectonics and basin subsidence history, *Geol. Soc. Am. Bull.* **121**, 55–64.

University of Washington
 Department of Earth and Space Sciences
 Box 351310
 Seattle, Washington 98195-1310

Manuscript received 25 April 2011

Queries

1. Journal style allows for 3 levels of subheads. The subheads in this section have been styled accordingly.
2. Data and Resources: What is the last date you accessed the website “<http://www.amath.washington.edu/~dgeorge/tsunamimodeling.html>”?
3. LeVeque (2008) reference: An Internet search revealed additional bibliographic data for this reference.
4. Please verify the accuracy of the author affiliation data.